Engineering Structures 133 (2017) 105–123

Contents lists available at ScienceDirect

Engineering Structures

journal homepage: www.elsevier.com/locate/engstruct

Seismic analysis and design of steel-plate concrete composite shear wall piers

Siamak Epackachi *, Andrew S. Whittaker, Amjad Aref

Dept. of Civil, Structural and Environmental Engineering, University at Buffalo, NY, United States

ARTICLE INFO

Article history:
Received 18 May 2016
Revised 12 December 2016
Accepted 13 December 2016

Keywords:
Steel-plate composite shear wall
Analytical model
Infill concrete
Steel faceplate
Mechanics-based equation
Statistical predictive models
LS-DYNA

ABSTRACT

This paper presents results of numerical studies on the in-plane monotonic response of steel-plate concrete (SC) composite shear wall piers. Results of finite element analysis of 98 SC wall piers are used to investigate the effects of wall aspect ratio, reinforcement ratio, slenderness ratio, axial load, yield strength of the steel faceplates, and uniaxial compressive strength of concrete on in-plane response, and to formulate (a) predictive equations to establish the trilinear lateral force versus lateral displacement response of SC wall piers up to peak strength, sufficient for seismic analysis of structures including SC wall piers and (b) a mechanics-based design equation for peak flexural strength, which addresses the interaction of co-existing shear and axial force. Design of Experiments is used to select the 98 piers. The baseline finite element model was formally validated using data from reversed cyclic, inelastic in-plane tests of four large-scale SC wall piers.

1. Introduction

Steel-plate concrete (SC) composite shear walls used or proposed for construction in the United States are constructed using steel faceplates, infill concrete, and connectors used to anchor the steel faceplates together and to the infill concrete. Although the seismic behavior of SC walls has been studied in some detail over the past 25+ years [1–20], the number of applications to date has been limited. Empirical equations to predict the initial stiffness and lateral load capacity of SC walls have been proposed, but effects of key design variables, including wall aspect ratio, reinforcement and slenderness ratios, axial load, and material properties have not been systemically accounted for. Herein, these design variables are addressed explicitly to

- Develop predictive equations to fully characterize the trilinear seismic response of an SC wall pier up to peak strength, suitable for inclusion in an analysis standard.
- Verify and validate a mechanics-based equation for the peak flexural strength of an SC wall pier, suitable for inclusion in a seismic design standard.

The following sections of this paper provide the technical bases for the predictive equations to characterize trilinear response and the mechanics-based equation for peak flexural strength. The literature review that follows immediately below focuses on those studies that address the behavior of SC wall piers considering one or more of the key design variables listed above.

2. Literature review

Fukumoto et al. [21] tested 1/4-scale steel plate, plain concrete, and composite shear walls under axial and shear loads to study the effects of composite action between the steel faceplates and the infill concrete, slenderness ratio, and stiffening methods for the steel faceplates, on the response of SC walls. The composite walls were constructed by assembling welded steel boxes and infilling them with concrete: different from the construction discussed above. Qualitative conclusions were drawn but they were by-and-large specific to the construction used.

Takeda et al. [22] subjected seven composite wall panels to in-plane cyclic loading in pure shear. The primary focus of their study was the effect of thickness of steel faceplates, partitioning webs, and the use of studs, on the shear response of SC panels. The specimens were composed of two steel faceplates, infill concrete, headed steel studs anchoring the faceplates to the infill, and the partitioning webs joining the steel faceplates: somewhat different to the construction discussed above. The results of the

* Corresponding author.
E-mail address: siamakep@buffalo.edu (S. Epackachi).

http://dx.doi.org/10.1016/j.engstruct.2016.12.024
0141-0296/

Nomenclature

A_c	cross-section area of infill concrete
A_c^{eff}	effective cross-sectional area of the infill concrete (= $A_c/1.2$)
A_g	total cross-section area of SC wall
A_s	cross-section area of steel faceplates
A_s^{eff}	effective cross-sectional area of the steel faceplates (= $A_s/1.2$)
c	depth to the neutral axis of the steel faceplates
c'	depth to the neutral axis of the infill concrete
E_c	elastic modulus of concrete (MPa)
E_s	elastic modulus of steel (MPa)
f'_c	uniaxial compressive stress of concrete (MPa)
f_t	nominal tensile strength of concrete (MPa)
f_t^*	effective tensile strength of concrete (MPa)
f_y	yield stress of steel faceplates (MPa)
f_s^*	effective stress in steel faceplates (MPa)
G_c	elastic shear modulus of concrete (MPa)
G_f	specific fracture energy (the energy required to propagate a tensile crack of unit area)
G_s	elastic shear modulus of steel (MPa)
H	wall height
H^*	moment to shear ratio (= wall height for single story wall panels)
I_c	moment of inertia of the cross section of the infill concrete
I_s	moment of inertia of the cross section of the steel faceplates
K_{el}	theoretical initial stiffness of SC wall
K_{el}^c	theoretical initial stiffness of infill concrete
K_{el}^s	theoretical initial stiffness of steel faceplates
K_{fc}	flexural stiffness of infill concrete
K_{vc}	shear stiffness of infill concrete
K_{fs}	flexural stiffness of steel faceplates
K_{vs}	shear stiffness of steel faceplates
K_{el}^s	theoretical initial stiffness of steel faceplates
K_y	pre-yield stiffness of SC wall
K_P	post-yield stiffness of SC wall
L	length of wall
M	bending moment
N	axial load
V_c^y	shear force resisted by infill concrete at the onset of steel faceplate yielding
V_s^y	shear force resisted by steel faceplates at the onset of steel faceplate yielding
V_y	lateral force resisted by SC wall at the onset of steel faceplate yielding
V_c^p	shear force resisted by infill concrete at peak lateral load
V_s^p	shear force resisted by steel faceplates at peak lateral load
V_p	lateral load capacity of SC wall
V_{flex}^*	shear force associated with the ultimate moment capacity of SC wall cross-section
t_c	thickness of infill concrete
t_s	thickness of each steel faceplate
w	crack width
ε_c	concrete strain at extreme fiber in compression
ε_{cu}	ultimate concrete strain
ε_y	steel strain at yielding
ρ_s	reinforcement ratio
β_1	stress block coefficient
β_2	stress block coefficient

Takeda study indicated that stud spacing, in the range considered, had no effect on peak strength. These authors parsed the pre-peak-strength response into four regions: (1) elastic, (2) post-concrete cracking, (3) post-buckling of steel faceplates, and (4) post-yielding of steel faceplates. The shear response of these SC panels was idealized using a perfectly plastic force-displacement relationship because their lateral load capacity did not deteriorate at shear strains less than 2%.

Sasaki et al. [23] tested seven flanged walls with aspect ratios ranging between 0.33 and 0.5 to investigate the effects of aspect ratio, reinforcement ratio, axial load, and the use of headed studs attached to the end plates of the web wall on the flexural-shear response of SC walls. A faceplate slenderness ratio of 33 was used. They reported the lateral stiffness and strength of a flanged SC walls increase with decreasing shear span-to-depth ratio and increasing reinforcement ratio, which is somewhat intuitive. Increases in axial load led to an increase in lateral strength but not initial stiffness.

Ozaki et al. [14] tested flanged walls with different aspect and reinforcement ratios under lateral loading to investigate the in-plane response of shear-critical and flexure-critical SC walls. Five shear-critical SC specimens with aspect ratios ranging from 0.5 to 0.85 and reinforcement ratios ranging from 0.7% to 2% were tested. The reinforcement ratio had a small effect on the initial stiffness and cracking strength of the shear-critical SC walls but it significantly affected the yield and the peak lateral loads. The displacements corresponding to the yield and lateral loads were not affected by reinforcement ratio. Four flexure-critical SC walls with aspect ratios of 0.7 and 0.85, and a reinforcement ratio of 2%, were also tested. The design parameters considered in this part of their study were aspect ratio, axial force, and type of SC wall connection to the foundation. Ozaki et al. proposed that the bending strength of flexure-critical SC walls be calculated using the results of plastic cross-section analysis. The interaction of axial force and bending moment was ignored.

Nie et al. [24] subjected twelve walls to axial and cyclic lateral loads to investigate the effects of reinforcement ratio, concrete strength, thicknesses of the steel face and flange plates, concrete reinforcement, and wall aspect ratio on the in-plane response of SC walls. The reinforcement and aspect ratios varied from 4.6% to 7.1%, and from 1 to 2, respectively. The twelve specimens failed in flexure, characterized by local buckling and fracture of the steel faceplates. Their test results showed that peak strength increased as shear span-to-depth ratio decreased. Changes in the concrete compressive strength had little effect on the stiffness of the SC specimens.

Kurt et al. [12] reported the effects of wall aspect ratio, wall thickness, and reinforcement ratio on the monotonic response of SC wall piers. The finite element codes ABAQUS [25] and LS-DYNA were used for the numerical simulations. Data from tests of eight SC wall piers [10,12] and the numerical simulations were used to derive design equations for the lateral load capacity of SC wall piers. The proposed equation for in-plane flexural capacity is parsed by aspect ratio (ratio of height to length): (1) for aspect ratios of 0.5 and smaller, the capacity is equal to the moment corresponding to the onset of yielding of the steel faceplates at the compression end of the wall and (2) for aspect ratios of 1.5 and greater, the capacity is equal to the plastic moment capacity of the wall cross-section. The flexural capacity for intermediate aspect ratios is determined by linear interpolation but accounts for wall thickness. The effects of co-existing axial and shearing forces on flexural capacity are not addressed.

3. Parametric study on SC wall piers

A research project was completed at the University at Buffalo in 2013 that investigated the seismic performance of SC composite wall piers for application to buildings and mission-critical infrastructure [8,10]. The SC walls considered in that study were composed of two steel faceplates and infill concrete: the construction introduced at the beginning of this paper. The steel faceplates were connected together and to the infill concrete using tie rods and headed studs, respectively. The research project, including an experimental program followed by numerical and analytical studies, focused on the in-plane behavior of flexure- and flexure-shear-critical SC wall piers. In the experimental program, four large-size specimens with an aspect ratio (height-to-length) of 1.0 were tested under displacement-controlled cyclic loading. The design variables were wall thickness, reinforcement ratio, and slenderness ratio. The walls were flexure-critical. A robust finite element model was developed in LS-DYNA for the simulation of the reversed cyclic, inelastic in-plane behavior of the flexure-critical SC walls [26]. The LS-DYNA model was formally validated for in-plane response calculations using the results of cyclic tests of SC wall piers. The test data also were used to develop simplified analytical models suitable for preliminary analysis and design of SC walls [11]. In the study reported in this paper, this validated LS-DYNA model for reversed cyclic, inelastic in-plane loading is used to conduct a parametric study on the in-plane monotonic response of SC walls. The results of the parametric study are used to systematically investigate the effects of design variables on the monotonic response of SC wall piers and to derive equations that characterize the trilinear lateral force-displacement relationship for an SC wall pier, all as described below.

The design variables considered in this study are: wall aspect ratio (AR), reinforcement ratio (RR), slenderness ratio of the steel faceplates (SR), axial load ratio (AL), yield strength of the steel faceplates (SS), and concrete compressive strength (CS). The reinforcement ratio is defined as the ratio of the cross-sectional area of the steel faceplates to the total cross-sectional area of SC wall. The faceplate slenderness ratio is the spacing of the connectors (studs or tie rods) divided by the steel faceplate thickness. The axial load ratio is the ratio of the applied axial compressive force to the product of the concrete compressive strength and the total wall area (i.e., $(2t_s + t_c)L$).

Information on the finite element analysis, and the results of the Analysis of Variance (ANOVA), and derivations of the predictive equations are presented in the following sub-sections.

4. Finite element analysis of SC walls

The general purpose finite element code LS-DYNA [27,28] was used to conduct the numerical study. The validated numerical model of the SC wall pier for calculations of reversed cyclic, inelastic in-plane response is summarized below. Detailed information on the finite elements, mesh sizes and related convergence studies, and formulations adopted can be found in [9,26]. Two features of the model are (a) use of the Winfrith constitutive model that enables shear-force transfer across cracks, opening and closing of cracks, loss of strength and stiffness in the direction parallel to cracks, and tension stiffening and (b) a contact algorithm to consider friction between the infill concrete and the steel faceplates, and to avoid penetration of concrete through steel, and vice versa, using a penalty-based approach.

The Winfrith concrete model in LS-DYNA (MAT085), developed by Broadhouse [26], was used for the infill concrete. In this study, three levels (i.e., low-, intermediate-, and high-levels) were considered for the yield strength of the steel faceplates and concrete compressive strength. Concrete compressive strengths of 27.5 MPa, 42 MPa, and 55 MPa were used to represent low, intermediate, and high values of compressive strength, respectively. The material properties for the concrete compressive strengths input to the LS-DYNA model are presented in Table 1. Young's modulus for concrete was calculated using Eq. (19.2.2.1(b)) of ACI 318-14 [29]: $4700\sqrt{f'_c}$. The tensile strength and fracture energy of the concrete were calculated per Sections 2.1.3.3.1 and 2.1.3.3.2 of [30], respectively, assuming an aggregate size of 19 mm for all concrete grades. The crack width was calculated as $2G_f/f_t$.

The Piecewise-Linear-Plasticity model in LS-DYNA (MAT024) was used for the steel faceplates and connectors. Plate steel of ASTM A36 ($f_y = 235$ MPa), A588 ($f_y = 350$ MPa), and A852 ($f_y = 460$ MPa) were used to represent low, intermediate, and high values of yield strength, respectively. Fig. 1 presents the stress-strain relationships assumed for the ASTM A36, A588, A852 steels used for the steel faceplates. The nominal yield and ultimate strengths of the studs and tie rods were assumed to be 345 and 450 MPa, respectively, and not varied for the analysis. The material properties input to LS-DYNA for the different grades of steel are presented in Table 2.

Studies in the literature report values for the coefficient of friction between steel and concrete between 0.2 and 0.7 (e.g., [31–34]). Of these studies, the second is the most relevant to the studies reported here. Rabbat et al. [32], tested 15 concrete blocks cast on steel plates: similar to the SC wall construction investigated here. Their results indicated that the coefficient of friction between flat steel and cast-in-place concrete varied between 0.57 and 0.7. Herein, the coefficient of friction between the steel faceplates and infill concrete was set to the lowest value in the range (= 0.57) of Rabbat et al. Importantly, the effect of friction between steel faceplates and infill concrete on the in-plane global response of SC wall piers was previously shown by the authors [26] to be negligible, because the normal stresses acting on the interface were tiny.

The CONTACT-AUTOMATIC-SURFACE-TO-SURFACE formulation available in LS-DYNA [27] was used to model the friction between the infill concrete and the steel faceplates. The CONSTRAINED-LAGRANGE-IN-SOLID formulation available in LS-DYNA [27] was used to tie the studs and tie rods to the infill concrete elements.

The studs and tie rods were modeled using beam elements. The infill concrete and the steel faceplates were modeled using $25.4 \times 25.4 \times 25.4$ mm eight-node solid elements and 25.4×25.4 mm four-node shell elements, respectively [9,26]. The constant stress formulation (ELFORM = 1 in LS-DYNA [27] and Belytschko-Tsay formulation are used for solid elements and shell elements, respectively. The cross section integrated beam element (Hughes-Liu beam in LS-DYNA [27]) is used for the connectors. The LS-DYNA models of the SC walls are presented in Fig. 2.

The length and the thickness of the walls were set to 1524 mm and 304.8 mm, respectively, to enable comparison with experimental results [8–10]. The heights of the SC walls were selected to achieve the targeted aspect ratios, ranging from 0.3 to 3.0.

5. Parametric study of SC walls using ANOVA

A Design of Experiments (DOE) [35] was used to effectively and efficiently explore the effects of the above-mentioned design variables on in-plane response of SC wall piers and to develop a trilinear lateral force-displacement relationship that will enable the seismic analysis of structures incorporating such piers. Fig. 3 is a geometrical representation of two- and three-level full factorial design together with a face-centered central composite design of three factors A, B, and C.

Table 1
Concrete material properties.

Compressive strength level	Young's modulus (MPa)	Poisson's ratio	Uniaxial compressive strength (MPa)	Uniaxial tensile strength (MPa)	Crack width (mm)	Agg. size (mm)
Low	24,856	0.20	27.6	2.8	0.052	19
Intermediate	30,442	0.20	41.4	3.6	0.052	19
High	35,151	0.20	55.2	4.4	0.053	19

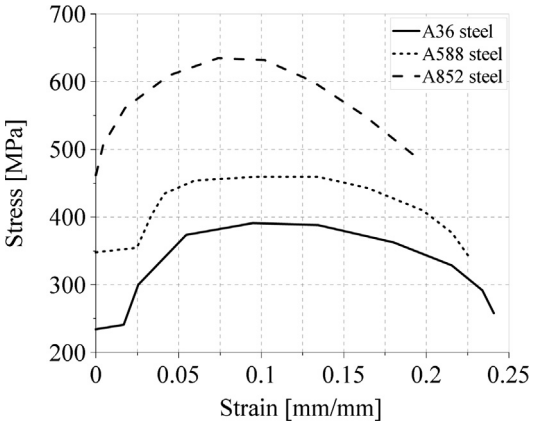

Fig. 1. Stress-strain relationships for the steel material.

Two-level full factorial design (Fig. 3a) is often used since it requires the least number of simulations for a problem with many design variables [35]. However, a two-level factorial design assumes that response is linear over the range of the design variables considered in the analysis. This assumption may not be applicable for the systems with nonlinear response [35]. In this study, a three-level, six-factor, fractional factorial design was used to build different combinations of the design variables: built using a face-centered central composite design (Fig. 3b) augmented by face-centered axial and center points (shown in Fig. 3b) to a two-level six-factor full factorial design. The central composite design, which consists of a two-level full factorial design with 2^{ψ} runs, where ψ is the number of factors, 2ψ axial runs, and n_c center runs, is used to build second-order response surface models avoiding the need to run a three-level full factorial experiment (Fig. 3c). The central composite design method efficiently considers the effects of the first- (e.g., $x_1, x_2, \ldots, x_n$) and second-order terms (e.g., $x_1^2, x_2^2, \ldots, x_n^2$) on the response.

Three levels (i.e., low-, intermediate-, and high-levels) are considered for each design variable. The levels of the design parameters used in the numerical analysis are presented in Table 3. The values in parentheses show the coded values used in the analysis; the low, intermediate, and high levels of the factors are denoted by −1, 0, and +1, respectively.

5.1. Analysis results

Key analysis results are summarized in Table 4. The levels of the design variables for each run are listed in columns 2–7. Columns 8–10 present the shear force resisted by the infill concrete and the steel faceplates, and the pre-yield stiffness of the SC walls at the onset of the steel faceplate yielding. Columns 11–13 list the contributions of the infill concrete and the steel faceplates to the total lateral load capacity and the post-yield stiffness of the SC walls. The pre-yield stiffness is the secant stiffness established at the force corresponding to the onset of the yielding of the steel faceplates. The post-yield stiffness is the slope of a line segment passing through the yield and reference points, where the reference point is established at the peak shear force and at a displacement calculated using an equal-energy-based tri-linear idealization of the LS-DYNA-predicted force-displacement relationship.

The shear force, V_{flex}, listed in column 14 of Table 4, is the shear force associated with the plastic moment capacity of the cross-section calculated using the code XTRACT [36]. The calculations assumed perfect bond between the steel faceplates and the infill concrete, steel and concrete material properties per Tables 1 and 2 and Fig. 1, and ignore the co-existing axial force and shear force interaction, both of which affect plastic moment capacity. Column 15 presents the ratio of $(V_c^p + V_s^p)$ to V_{flex}. Values greater than 1.0 identify the shortcomings of the traditional assumptions used to compute moment capacity, including plane sections remaining plane after loading, and ignoring shear and axial force interaction.

5.2. Analysis of variance

An Analysis of Variance (ANOVA) was conducted using the commercial software Minitab [37] to investigate the main and interaction effects of the design variables on response. The results of ANOVA are presented in the following sub-sections.

5.2.1. Main effects

The average values of the response variables at the low and high levels of the design variables are presented in Fig. 4. The plots identify the factors that have a significant effect on the response of SC walls: as the slope of the line increases, the main effect of the design variables increases [35]. Fig. 4 shows that the aspect ratio (AR) has a significant effect on the yield and peak shear load and on the pre- and post-yield lateral stiffness. The negative slope in these panels delineates that as the aspect ratio increases, the lateral strength and stiffness of SC walls decrease.

Fig. 4 also indicates that reinforcement ratio (RR) has a greater effect on strength than stiffness because the slope of the RR line in the plots for V_y and V_p is greater than in those for K_y and K_p, whereas the slenderness ratio (SR) has no effect on V_y and only a small effect on V_p and K_y, the post-yield stiffness is markedly influenced by slenderness ratio. As the faceplate slenderness ratio increases, the post-yield stiffness decreases, which is an expected

Table 2
Steel material properties.

Yield strength level	Young's modulus (MPa)	Poisson's ratio	Yield strength (MPa)	Ultimate strength (MPa)	Fracture strain (%)
Low	200,000	0.30	235	390	24
Intermediate	200,000	0.30	350	460	22
High	200,000	0.30	460	635	19

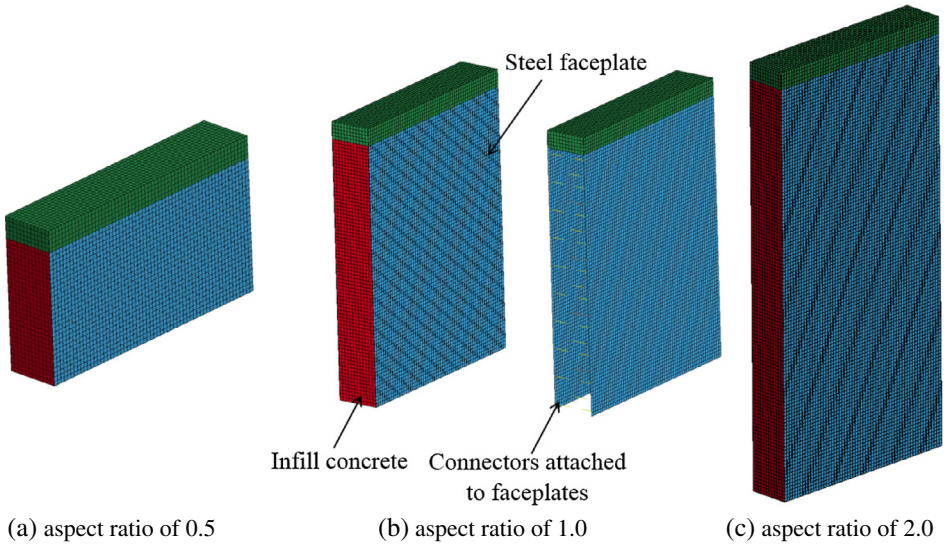

Fig. 2. LS-DYNA model.

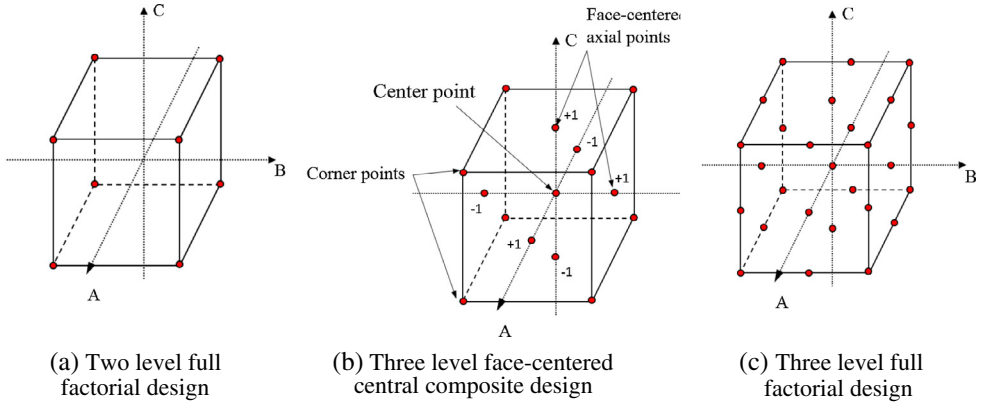

Fig. 3. Three factor factorial design.

Table 3
Levels of the design parameters.

Variable	Low	Intermediate	High
Aspect ratio	0.5 (−1)	1.25 (0)	2.0 (+1)
Reinforcement ratio (%)	1.67 (−1)	3.33 (0)	5.0 (+1)
Slenderness ratio	10 (−1)	25 (0)	40 (+1)
Axial load ratio	0 (−1)	0.1 (0)	0.2 (+1)
Yield strength of the steel faceplates (MPa)	235 (−1)	350 (0)	460 (+1)
Concrete compressive strength (MPa)	27.6 (−1)	41.4 (0)	55.2 (+1)

result because as the slenderness ratio increases, buckling of the steel faceplates and the onset of loss of stiffness occur earlier.

Fig. 4 also shows that the axial load ratio (AL), concrete compressive strength (CS), and steel yield strength (SS) have approximately the same effect on the yield and lateral load capacities of SC walls. However, an increase in the axial load and concrete compressive strength increase the pre- and post-yield stiffness but they decrease as the steel yield strength increases.

5.2.2. Interaction effects

The interaction plots of the design variables are presented in Fig. 5. There is significant interaction between two variables if the effect of one variable on the response substantially changes for different values of another variable. Parallel lines in an interaction plot indicate that there is no interaction between the design variables. As the difference in the slopes of the lines increases, the degree of the interaction between the design variables increases [35].

In Fig. 5, the cells in the first row of plots in each panel present the degree of interaction between aspect ratio and the other design variables. The greater the difference in the slopes of the two lines in each cell, the greater the interaction. For example, in the first row in panels (a) and (b), the lines are parallel in only one cell (AR + SR: second cell from the left), indicating that significant interaction of AR with RR, AL, SS and CS, but not with SR, in the calculation of V_y and V_p.

Fig. 5b and d indicates that there is an interaction between reinforcement ratio and slenderness ratio, which influences the estimation of V_p and K_p. This interaction is attributed to the fact that any change in the reinforcement ratio, for a constant wall thickness, changes the steel faceplate thickness and the slenderness ratio. There is also interaction between axial load and concrete compressive strength because the applied compressive load is a fraction (0, 0.1, 0.2) of the product of the concrete compressive strength and the cross-sectional area of the wall ($A_g f'_c$). The axial load interacts with the yield strength of the steel faceplates in the calculation of K_p. An increase in the steel strength slightly

Table 4
LS-DYNA and cross-sectional analysis results.

Run	Factor levels						Data at yield point			Data at peak point			Cross-sectional analysis	
	AR	RR	SR	AL	SS	CS	V_c^y (kN)	V_s^y (kN)	K_y (kN/mm)	V_c^p (kN)	V_s^p (kN)	K_p (kN/mm)	V_{flex} (kN)	$\frac{V_c^p+V_s^p}{V_{flex}}$
(1)	(2)	(3)	(4)	(5)	(6)	(7)	(8)	(9)	(10)	(11)	(12)	(13)	(14)	(15)
1	−1	−1	−1	−1	−1	−1	965	227	3069	1646	641	1357	1601	1.43
2	−1	−1	−1	−1	−1	+1	1419	240	4260	2224	627	1833	1686	1.69
3	−1	−1	−1	−1	+1	−1	1552	645	1909	1917	1388	1576	2865	1.15
4	−1	−1	−1	−1	+1	+1	2126	592	2656	2985	1277	1916	3145	1.36
5	−1	−1	−1	+1	−1	−1	1962	369	3629	2535	801	2109	3132	1.06
6	−1	−1	−1	+1	−1	+1	3154	360	5471	4639	827	3106	5004	1.09
7	−1	−1	−1	+1	+1	−1	2371	725	2691	2553	1615	1944	3954	1.05
8	−1	−1	−1	+1	+1	+1	4035	636	4563	4488	1592	3131	5921	1.03
9	−1	−1	+1	−1	−1	−1	1085	271	2626	1610	605	976	1601	1.38
10	−1	−1	+1	−1	−1	+1	1610	271	3652	2180	480	670	1579	1.69
11	−1	−1	+1	−1	+1	−1	1312	480	1999	1873	1339	936	2865	1.12
12	−1	−1	+1	−1	+1	+1	1939	480	2698	2829	1157	1321	3145	1.27
13	−1	−1	+1	+1	−1	−1	2117	405	3283	2402	765	1429	3132	1.01
14	−1	−1	+1	+1	−1	+1	3527	396	5100	4395	778	1656	5004	1.03
15	−1	−1	+1	+1	+1	−1	2406	707	2438	2264	1570	950	3954	0.97
16	−1	−1	+1	+1	+1	+1	4288	698	3906	4399	1294	1664	5921	0.96
17	−1	+1	−1	−1	−1	−1	1201	823	3921	2202	2024	2303	4110	1.03
18	−1	+1	−1	−1	−1	+1	1739	832	4989	3501	1886	2324	4537	1.19
19	−1	+1	−1	−1	+1	−1	1726	1619	3270	2718	4502	1889	6970	1.04
20	−1	+1	−1	−1	+1	+1	2277	1450	4158	4097	4137	2620	7740	1.06
21	−1	+1	−1	+1	−1	−1	2042	1237	4261	2527	2304	3103	5120	0.94
22	−1	+1	−1	+1	−1	+1	3403	1219	6003	4537	2286	3664	7055	0.97
23	−1	+1	−1	+1	+1	−1	2313	1913	3675	2776	4706	2146	7504	1.00
24	−1	+1	−1	+1	+1	+1	4168	2131	4931	4510	4791	2587	9186	1.01
25	−1	+1	+1	−1	−1	−1	1348	961	3596	2189	2037	2114	4110	1.03
26	−1	+1	+1	−1	−1	+1	1953	952	4521	3296	1922	2238	4537	1.15
27	−1	+1	+1	−1	+1	−1	1704	1552	3181	2540	4417	1950	6970	1.00
28	−1	+1	+1	−1	+1	+1	2429	1539	3875	3981	3848	2781	7740	1.01
29	−1	+1	+1	+1	−1	−1	2068	1174	4215	2473	2273	2603	5120	0.93
30	−1	+1	+1	+1	−1	+1	3421	1165	5958	4622	2295	3569	7055	0.98
31	−1	+1	+1	+1	+1	−1	2442	1988	3467	2527	4582	1891	7504	0.95
32	−1	+1	+1	+1	+1	+1	4221	1979	4856	4253	4599	2842	9186	0.96
33	+1	−1	−1	−1	−1	−1	240	67	151	307	200	43	400	1.27
34	+1	−1	−1	−1	−1	+1	329	67	221	387	178	42	396	1.43
35	+1	−1	−1	−1	+1	−1	249	182	95	556	409	57	716	1.35
36	+1	−1	−1	−1	+1	+1	298	209	142	716	329	60	787	1.33
37	+1	−1	−1	+1	−1	−1	507	111	194	663	249	81	783	1.17
38	+1	−1	−1	+1	−1	+1	983	102	271	1286	245	103	1250	1.22
39	+1	−1	−1	+1	+1	−1	445	187	107	863	463	66	988	1.34
40	+1	−1	−1	+1	+1	+1	1134	187	223	1419	480	85	1481	1.28
41	+1	−1	+1	−1	−1	−1	236	93	120	276	236	34	400	1.28
42	+1	−1	+1	−1	−1	+1	351	98	163	414	191	25	396	1.53
43	+1	−1	+1	−1	+1	−1	173	222	85	463	431	47	716	1.25
44	+1	−1	+1	−1	+1	+1	236	254	109	587	409	46	787	1.27
45	+1	−1	+1	+1	−1	−1	547	129	169	689	240	60	783	1.19
46	+1	−1	+1	+1	−1	+1	983	138	248	1272	236	76	1250	1.21
47	+1	−1	+1	+1	+1	−1	556	240	132	672	547	51	988	1.23
48	+1	−1	+1	+1	+1	+1	1045	249	198	1286	520	84	1481	1.22
49	+1	+1	−1	−1	−1	−1	316	254	190	592	658	92	1028	1.22
50	+1	+1	−1	−1	−1	+1	431	254	239	814	596	86	1134	1.24
51	+1	+1	−1	−1	+1	−1	436	494	160	867	1375	94	1744	1.29
52	+1	+1	−1	−1	+1	+1	520	489	192	1268	1299	108	1935	1.33
53	+1	+1	−1	+1	−1	−1	543	334	226	765	747	111	1281	1.18
54	+1	+1	−1	+1	−1	+1	939	360	305	1446	694	132	1761	1.21
55	+1	+1	−1	+1	+1	−1	636	609	191	930	1481	91	1877	1.28
56	+1	+1	−1	+1	+1	+1	1076	641	257	1650	1428	119	2295	1.34
57	+1	+1	+1	−1	−1	−1	245	289	164	423	752	77	1028	1.14
58	+1	+1	+1	−1	−1	+1	320	329	199	520	770	93	1134	1.14
59	+1	+1	+1	−1	+1	−1	262	578	139	556	1601	90	1744	1.24
60	+1	+1	+1	−1	+1	+1	258	658	158	787	1624	100	1935	1.25
61	+1	+1	+1	+1	−1	−1	480	396	206	636	823	108	1281	1.14
62	+1	+1	+1	+1	−1	+1	903	431	280	1259	787	117	1761	1.16
63	+1	+1	+1	+1	+1	−1	476	738	169	543	1793	89	1877	1.24
64	+1	+1	+1	+1	+1	+1	961	770	229	1143	1810	104	2295	1.29
65	0	0	0	0	0	0	992	476	624	1446	1157	273	1984	1.31
66	−1	0	0	0	0	0	2491	1005	3652	3345	2064	2406	4964	1.09
67	+1	0	0	0	0	0	311	289	149	743	556	72	1241	1.05
68	0	−1	0	0	0	0	1014	236	561	1254	556	154	1415	1.28
69	0	+1	0	0	0	0	992	756	670	1775	1584	249	2722	1.23
70	0	0	−1	0	0	0	1005	489	634	1597	1108	248	1984	1.36

Table 4 (*continued*)

Run	Factor levels						Data at yield point			Data at peak point			Cross-sectional analysis	
	AR	RR	SR	AL	SS	CS	V_c^y (kN)	V_s^y (kN)	K_y (kN/mm)	V_c^p (kN)	V_s^p (kN)	K_p (kN/mm)	V_{flex} (kN)	$\frac{V_c^p+V_s^p}{V_{flex}}$
(1)	(2)	(3)	(4)	(5)	(6)	(7)	(8)	(9)	(10)	(11)	(12)	(13)	(14)	(15)
71	0	0	+1	0	0	0	996	512	577	1517	1032	193	1984	1.29
72	0	0	0	−1	0	0	636	423	504	1197	970	160	1659	1.30
73	0	0	0	+1	0	0	1352	547	695	1842	1165	292	2402	1.25
74	0	0	0	0	−1	0	947	356	706	1312	796	270	1575	1.34
75	0	0	0	0	+1	0	1054	632	564	1637	1668	227	2398	1.38
76	0	0	0	0	0	−1	743	476	518	1112	1139	240	1721	1.31
77	0	0	0	0	0	+1	1241	507	705	1939	1032	219	2224	1.34

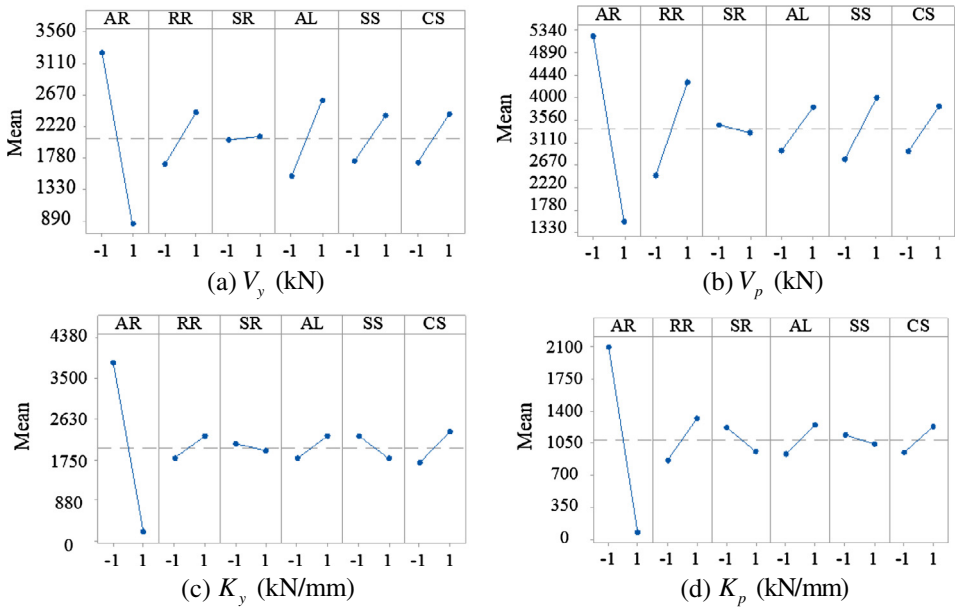

Fig. 4. Main effect plots of design variables.

increases K_p when there is no axial load but it significantly decreases K_p at an axial load of $0.2A_g f'_c$ (see Fig. 5d).

5.3. Empirical predictive equations for the monotonic response of SC wall piers

The pre-peak-strength response of SC wall piers can be approximated by a tri-linear force-displacement relationship, as presented in Fig. 6. Two stages of pre-peak response are assumed, namely, (1) pre-yielding and (2) post-yielding of the steel faceplates.

The yield load, V_y, and the lateral load capacity, V_p, of a SC wall pier can be calculated as the sum of the factored strengths of the infill concrete, $A_c f'_c$, and the steel faceplates, $A_s f_y$, as follows:

$$V_y = \alpha_c^y A_c f'_c + \alpha_s^y A_s f_y \tag{1}$$

$$V_p = \alpha_c^p A_c f'_c + \alpha_s^p A_s f_y \tag{2}$$

The pre- and post-yield stiffness of an SC wall pier, in the absence of foundation flexibility, can be calculated as:

$$K_y = \beta_y K_{el} \tag{3}$$

$$K_p = \beta_p K_{el} \tag{4}$$

where K_{el} can be calculated as:

$$K_{el} = K_{el}^c + K_{el}^s = \frac{1}{\frac{1}{K_{fc}} + \frac{1}{K_{vc}}} + \frac{1}{\frac{1}{K_{fs}} + \frac{1}{K_{vs}}} \tag{5}$$

The flexural and shear stiffness are calculated as:

$$K_{fc} = \frac{3E_c I_c}{H^3}, \quad K_{fs} = \frac{3E_s I_s}{H^3} \tag{6}$$

$$K_{vc} = \frac{G_c A_c^{eff}}{H}, \quad K_{vs} = \frac{G_s A_s^{eff}}{H} \tag{7}$$

The results of the finite element analyses were used to develop empirical equations to calculate the strength and stiffness factors α_c^y, α_s^y, α_c^p, α_s^p, β_y, and β_p. The factors α_c^y and α_s^y were calculated as the LS-DYNA-predicted shear forces resisted by the infill concrete and steel faceplates, respectively, at the onset of the steel faceplate yielding divided by the corresponding product of their compressive (yield) strengths and area. The factors α_c^p and α_s^p were calculated as the ratio of the contributions of the infill concrete and the steel faceplates to the lateral load capacity of SC wall, respectively, to the corresponding product of their compressive (yield) strengths and area. The factor β_y was calculated as the LS-DYNA-predicted normalized secant stiffness (i.e., secant stiffness divided by the theoretical initial stiffness) established at the force corresponding to the onset of the yielding of the steel faceplates. Factor β_p was esti-

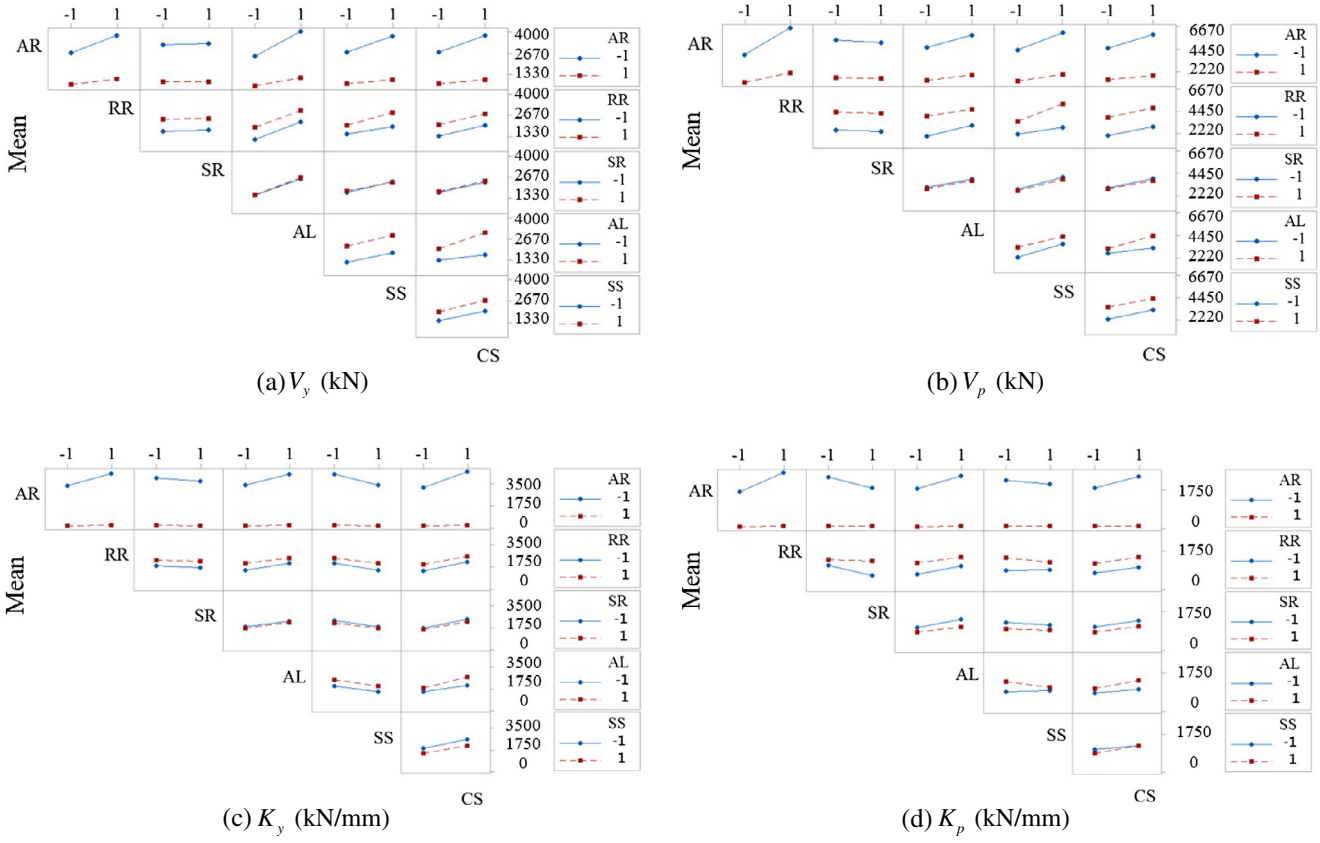

Fig. 5. Interaction plots of design variables.

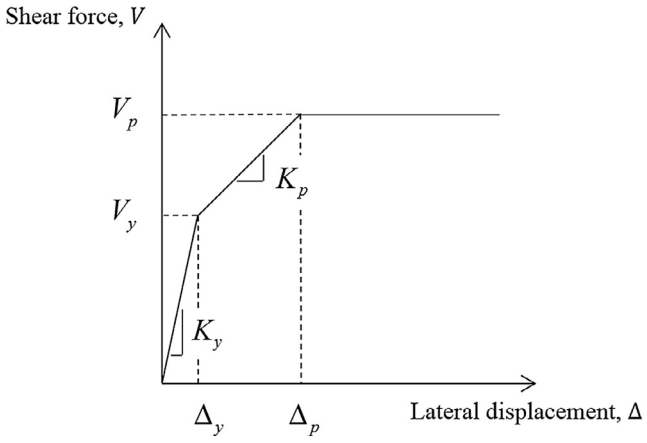

Fig. 6. Tri-linear shear force-displacement relationship.

mated as the slope of the line segment passing through the yield and reference points on the LS-DYNA-predicted force-displacement relationship.

The calculated strength and stiffness factors were subsequently used as an input for the ANOVA. The results of the ANOVA for α_c^p and α_s^p are presented in Table 5 including the sum of squares, percentage contribution, mean squares, F- and P-values for each item of the full quadratic terms including linear, square, and 2-way interaction terms.

The results of ANOVA for the other response factors α_c^y, α_s^y, β_y, and β_p are presented in Epackachi and Whittaker [9] and are not repeated here. The total sum of squares (SS) has N − 1 degrees of freedom (DF), where N is the number of the analyses (= 77). Considering full quadratic terms in the model, there are 27 terms with one degree of freedom for each term, where the degree of freedom for the main effect terms is the number of levels of the factor minus 1 and the degree of freedom of the interaction terms is calculated as the product of the degrees of freedom of the corresponding main effects. The percentage contribution, estimated as the ratio of the sum of squares for each term to the total sum of squares, shows the relative importance of each term used to predict the response variable. The mean squares calculated by dividing the sum of squares of each term to its corresponding degrees of freedom represent an estimate of the population variance. The F- and P-values in Table 5 represent the significance of each term on the response variable. The effects of the factors with a probability less than 5% (P-value less than 0.05) are considered to be significant on the response variable at the 95% confidence level. The results presented in Table 5 help to identify the terms with significant contributions (i.e., with a P-value less than 0.05) that need to be included in the regression model.

Table 6 lists the coefficients of the linear, square, and interaction terms of the regression equations for the response factors α_c^y, α_s^y, α_c^p, α_s^p, β_y, and β_p. The coefficient of each term estimates the change in the mean response per unit increase in that term when all other terms are held constant [35]. The regression equations also include a constant. The proposed equations are valid for the range of design variables presented in Table 3.

Each term in Table 3 is a coded parameter ranging between −1 and +1. The relationship between the coded and actual terms is:

$$y_c = 2\left(\frac{y_a - A}{B - A}\right) - 1 \tag{8}$$

where y_c and y_a are the coded and actual values of the variable, respectively, and A and B are the actual lower and upper limits on the variable, respectively.

Table 5
Results of ANOVA for α_c^p and α_s^p.

Var.	DF	Response factor α_c^p					Response factor α_s^p				
		Seq SS	Contr.	MS	F-Val.	P-Val.	Seq SS	Contr.	MS	F-Val.	P-Val.
Linear											
AR	1	0.2403	82.46%	0.2403	5082.8	0.00	1.1472	91.37%	1.1472	5947.8	0.00
RR	1	0.0051	1.75%	0.0051	107.6	0.00	0.0037	0.29%	0.0037	19.1	0.00
SR	1	0.0013	0.43%	0.0013	26.7	0.00	0.0001	0.01%	0.0001	0.6	0.43
AL	1	0.0169	5.80%	0.0169	357.2	0.00	0.0323	2.58%	0.0323	167.7	0.00
SS	1	0.0020	0.70%	0.0020	43.0	0.00	0.0026	0.21%	0.0026	13.4	0.00
CS	1	0.0061	2.08%	0.0061	128.1	0.00	0.0033	0.26%	0.0033	17.0	0.00
Square											
AR^2	1	0.0059	2.01%	0.0017	35.7	0.00	0.0302	2.41%	0.0042	21.5	0.00
RR^2	1	0.0000	0.00%	0.0000	0.1	0.82	0.0002	0.02%	0.0000	0.0	0.99
SR^2	1	0.0000	0.00%	0.0000	0.1	0.79	0.0001	0.00%	0.0000	0.1	0.79
AL^2	1	0.0000	0.00%	0.0000	0.0	0.86	0.0000	0.00%	0.0000	0.2	0.70
SS^2	1	0.0000	0.01%	0.0000	0.5	0.50	0.0015	0.12%	0.0015	7.7	0.01
CS^2	1	0.0000	0.00%	0.0000	0.1	0.74	0.0000	0.00%	0.0000	0.0	1.00
2-Way interaction											
AR × RR	1	0.0015	0.50%	0.0015	30.7	0.00	0.0000	0.00%	0.0000	0.0	0.91
AR × SR	1	0.0000	0.01%	0.0000	0.8	0.37	0.0061	0.49%	0.0061	31.6	0.00
AR × AL	1	0.0018	0.63%	0.0018	38.9	0.00	0.0096	0.76%	0.0096	49.7	0.00
AR × SS	1	0.0001	0.02%	0.0001	1.4	0.24	0.0005	0.04%	0.0005	2.4	0.13
AR × CS	1	0.0020	0.69%	0.0020	42.6	0.00	0.0009	0.07%	0.0009	4.4	0.04
RR × SR	1	0.0002	0.06%	0.0002	3.4	0.07	0.0019	0.15%	0.0019	9.6	0.00
RR × AL	1	0.0032	1.09%	0.0032	67.0	0.00	0.0026	0.20%	0.0026	13.3	0.00
RR × SS	1	0.0000	0.01%	0.0000	0.5	0.47	0.0004	0.03%	0.0004	1.9	0.18
RR × CS	1	0.0001	0.03%	0.0001	1.6	0.21	0.0003	0.02%	0.0003	1.4	0.24
SR × AL	1	0.0000	0.01%	0.0000	0.5	0.47	0.0000	0.00%	0.0000	0.1	0.77
SR × SS	1	0.0003	0.10%	0.0003	5.9	0.02	0.0000	0.00%	0.0000	0.0	0.88
SR × CS	1	0.0001	0.03%	0.0001	1.7	0.21	0.0003	0.03%	0.0003	1.7	0.20
AL × SS	1	0.0015	0.50%	0.0015	30.9	0.00	0.0008	0.07%	0.0008	4.3	0.04
AL × CS	1	0.0008	0.28%	0.0008	17.3	0.00	0.0013	0.11%	0.0013	6.9	0.01
SS × CS	1	0.0001	0.02%	0.0001	1.5	0.23	0.0002	0.02%	0.0002	1.2	0.28
Model	27	27	0.2891	99.21%	0.2891	226.5	27	1.2461	99.25%	0.0462	239.3
Error	49	49	0.0023	0.79%			49	0.0095	0.75%		
Total	76	76	0.2914	100.00%			76	1.2555	100.00%		

Table 6
Coefficients of the regression models for the response variables.

α_s^y		α_c^y		α_s^p		α_c^p		β_y		β_p	
Term	Coeff.	Term	Coeff.	Term	Coeff.	Term	Coeff.	Term	Coeff.	Term	Coeff.
Cons.	0.0914	Cons.	0.0522	Cons.	0.2018	Cons.	0.0790	Cons.	0.5909	Cons.	0.2215
AR	−0.0591	AR	−0.0487	AR	−0.1318	AR	−0.0603	AR	0.0099	AR	−0.0291
RR	0.0014	RR	0.0027	RR	0.0075	RR	0.0088	RR	0.0189	RR	0.0414
SR	0.0038	SR	0.0002	SR	−0.0014	SR	−0.0044	SR	−0.0295	SR	−0.0299
AL	0.0164	AL	0.0229	AL	0.0221	AL	0.0160	AL	0.0780	AL	0.0431
SS	−0.0033	SS	0.0071	SS	0.0063	SS	0.0055	SS	−0.0752	SS	−0.0073
AR^2	0.0262	CS	−0.0081	CS	−0.0071	CS	−0.0096	CS	0.0137	CS	−0.0113
AR × SR	0.0026	AR^2	0.0248	AR^2	0.0391	AR^2	0.0249	AR^2	0.0037	AR^2	0.0705
AR × AL	−0.0100	AR × RR	−0.0017	SS^2	0.0223	AR × RR	−0.0048	AR × SR	−0.0096	AR × SR	0.0117
AR × SS	0.0038	AR × SR	−0.0020	AR × SR	0.0098	AR × AL	−0.0054	AR × AL	0.0113	AR × SS	0.0077
RR × SS	−0.0042	AR × AL	−0.0116	AR × AL	−0.0122	AR × CS	0.0056	RR × AL	−0.0140	RR × SR	0.0214
SR × SS	−0.0028	AR × SS	−0.0066	AR × CS	0.0037	RR × AL	−0.0070	RR × SS	0.0195	RR × AL	−0.0124
AL × SS	−0.0046	AR × CS	0.0058	RR × SR	0.0054	SR × SS	−0.0021	RR × CS	−0.0119	RR × SS	−0.0107
		RR × AL	−0.0026	RR × AL	−0.0063	AL × SS	−0.0048	SR × SS	0.0095	SR × AL	−0.0075
		SR × SS	−0.0015	AL × SS	−0.0036	AL × CS	0.0036	AL × CS	0.0187	AL × SS	−0.0230
		AL × CS	0.0014	AL × CS	0.0046					AL × CS	0.0098
										SS × CS	0.0097

5.4. Adequacy of the regression models

In an analysis of variance, the regression model is developed assuming that the errors are normally and independently distributed with a mean of zero. The validity of this assumption and the model adequacy can be investigated by examining the residuals, where the residual is defined as the difference between the measured and model-predicted value of the response variable. The regression model is adequate if the residuals are structureless and normally distributed [35].

The normal probability of the residuals and the LS-DYNA-predicted response variables versus residuals are presented in Fig. 7. The residuals of the response variables, presented in the left panels of Fig. 7, are linear, indicating that the distribution of the residuals is normal. The plots of residuals versus response variables presented in the right panels of Fig. 7 investigate the independence

assumption in the analysis of variance. As seen in Fig. 7, the plots of the residuals versus the response variables are random and structureless, indicating that the assumption of independence is valid.

6. Mechanics-based equations for predicting peak flexural strength

Experimental and numerical investigations on the in-plane seismic response of SC wall piers [10,12,38] have made it clear that behavior is governed by flexure unless the aspect ratio is much less than 0.5. Flexural (and thus shear) capacity is limited by buckling of the steel faceplates at the free vertical edges of the wall. The significant interaction of shear and axial forces, and bending moment, on lateral load capacity of SC wall piers shown above makes it clear that strength-based predictive equations ignoring coupled behavior may be substantially inaccurate and lead to unconservative designs. Herein, the interactions between shear and axial force, and bending moment, are considered in the derivation of equations for in-plane flexural capacity of SC walls that could be implemented in a design standard. The lateral capacity of an SC walls can be calculated by dividing its flexural capacity by its moment-to-shear ratio (or the height in a single story wall panel).

The derivation of mechanics-based equations for composite systems, which address the interaction of key design variables, utilizes insight gained from finite element analysis of validated models. A parametric study was conducted considering aspect ratios ranging from 0.3 to 3.0, reinforcement ratios ranging from 1.6% to 6.6%, and axial load ratio ranging from 0 to 0.2 m, where these terms were described previously. ASTM A36 steel was assumed

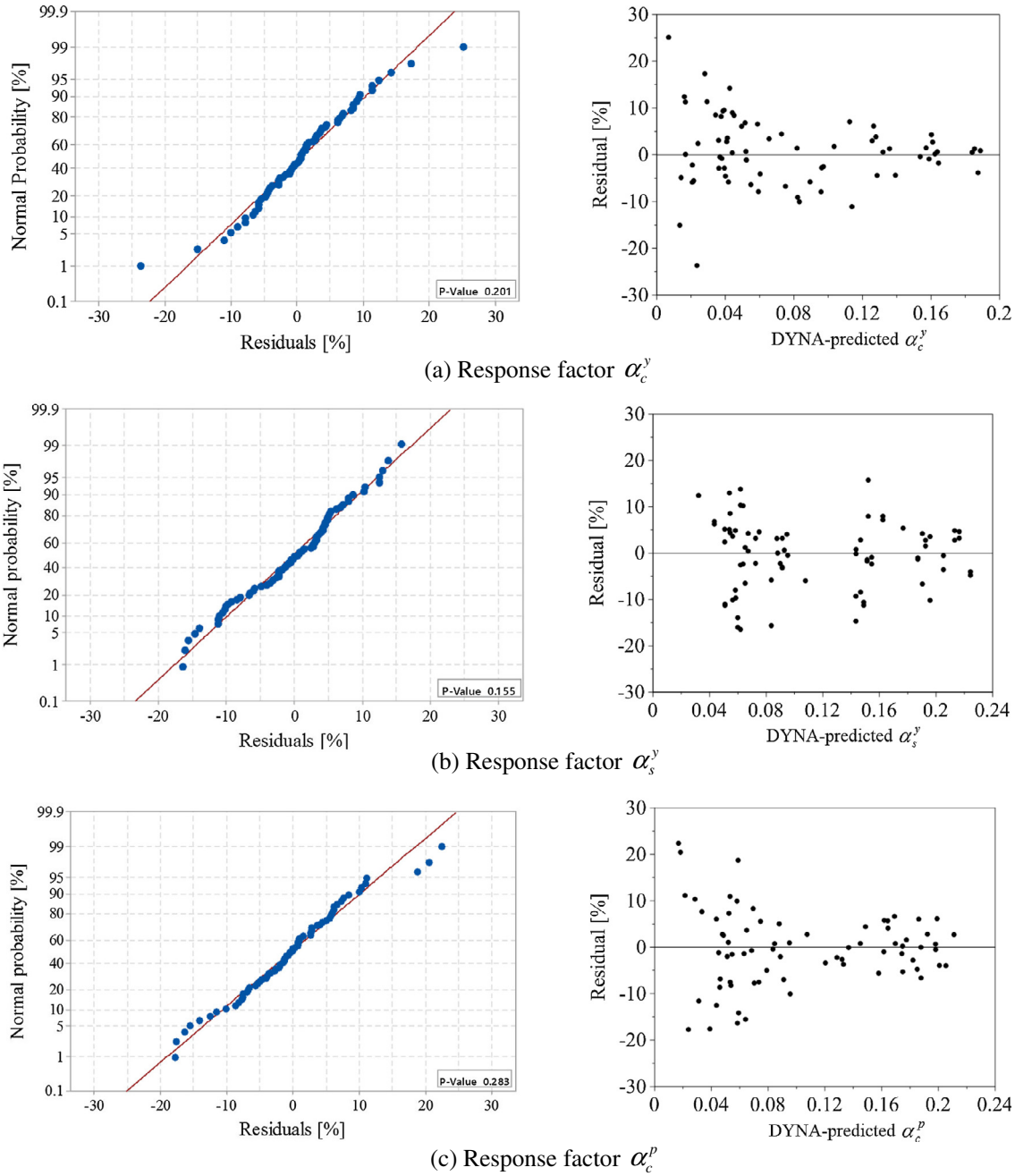

Fig. 7. Plots of normal probability versus residual (left) and residual versus LS-DYNA-predicted response variable (right).

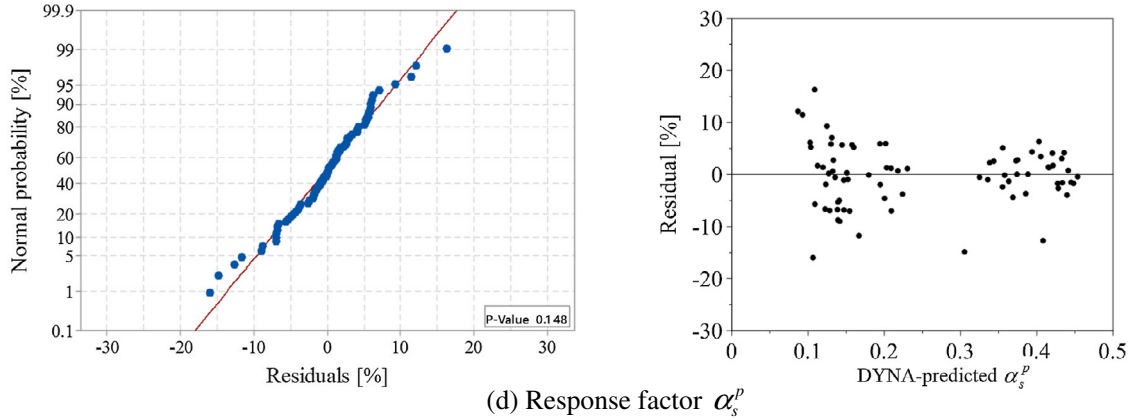

(d) Response factor α_s^p

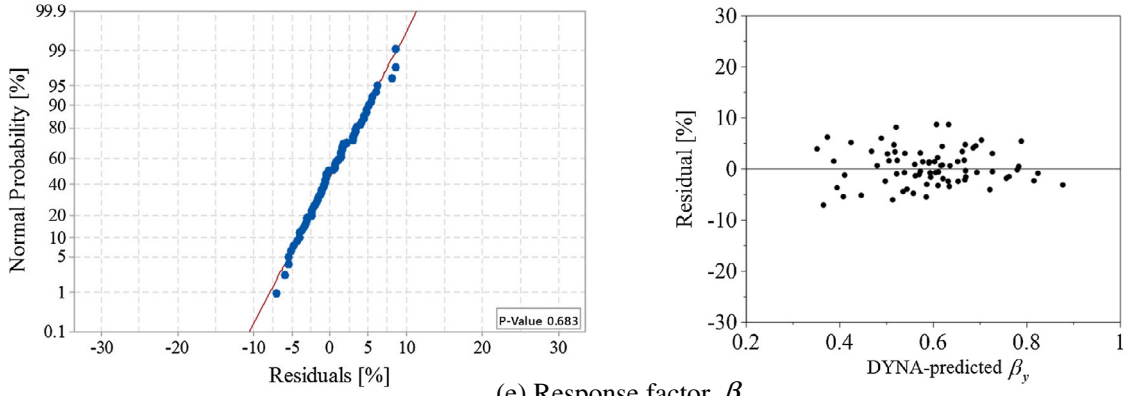

(e) Response factor β_y

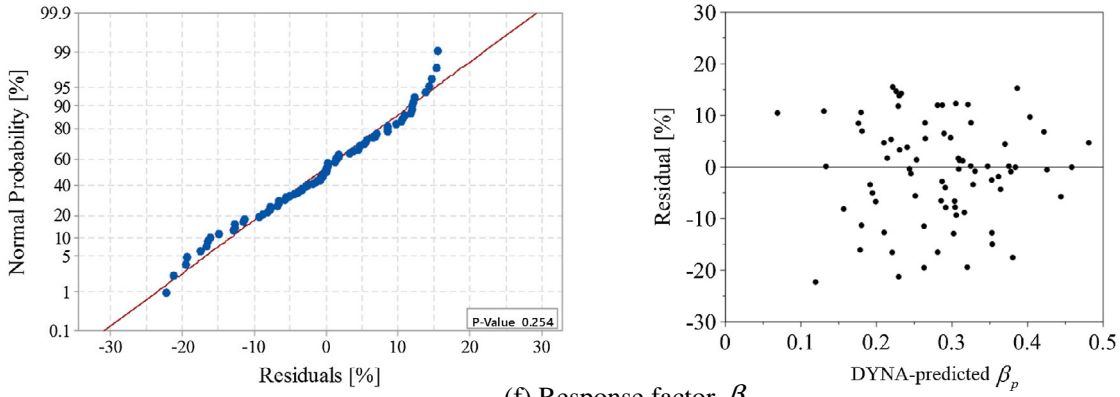

(f) Response factor β_p

Fig. 7 (*continued*)

for the steel faceplates, with values of the yield and tensile strengths of 262 and 380 MPa, respectively. The compressive strength of the infill concrete was assumed to be 27.5 MPa. The length and thickness of the wall models were the same as the 77 models used for derivation of the ANOVA-based equations. The material models, element types, boundary conditions, and loading were the same as those discussed previously.

6.1. Analysis results

Fig. 8 presents the variation of the averaged normal stress in the steel faceplates and in the infill concrete at peak lateral resistance for the SC walls with aspect ratios ranging from 0.3 to 3. As seen in Fig. 8, the vertical stress profiles in the steel faceplates and infill concrete are significantly affected by shear-flexure interaction for walls with aspect ratios of less than 1.5. As aspect ratio decreases, the shear stress increases and the extent of yielding on the tension side of the steel faceplates decreases. Fig. 8 shows that the neutral axis for the steel faceplates and the infill concrete are not collocated for walls with an aspect ratio of less than 1.5, noting that the distance between the neutral axes decreases as the aspect ratio increases. Fig. 8 also indicates that the maximum tensile and compressive strain at the wall ends increase as the aspect ratio increases and the extent of yielding on the compression side of the steel faceplates increases. As seen in Fig. 8, the tensile stress in the infill concrete decreases as the aspect ratio increases.

The effect of axial load on the vertical stress profiles in the steel faceplates and the infill concrete is presented in Fig. 9. As the axial

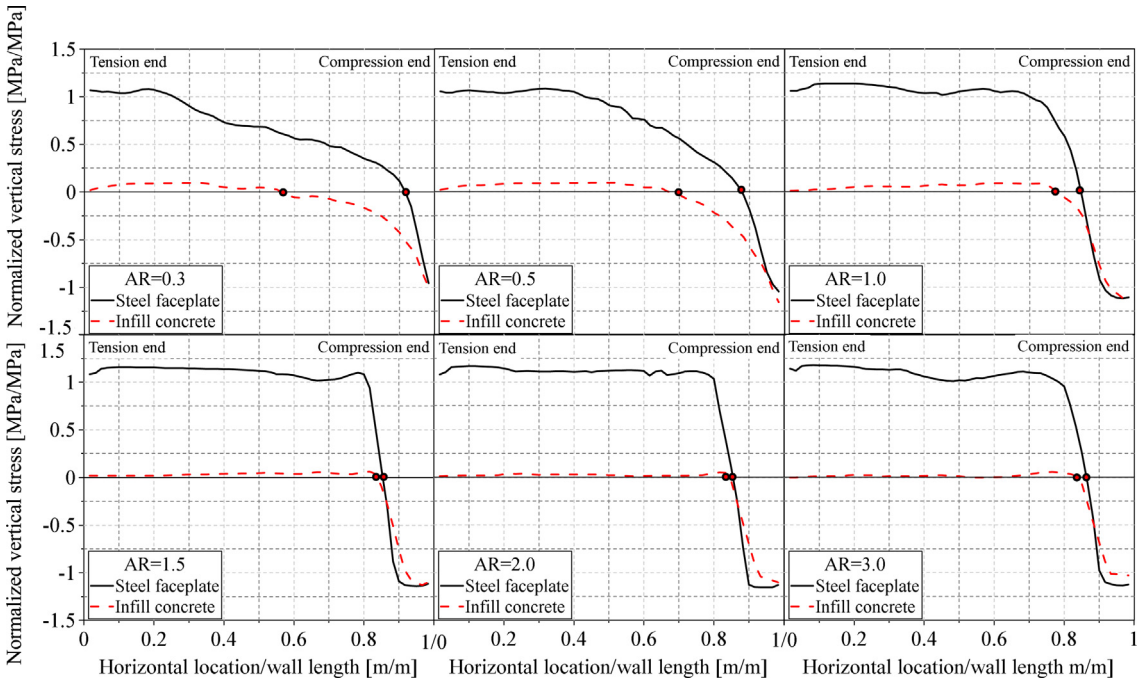

Fig. 8. DYNA-predicted normal stress in steel faceplates and infill concrete at peak lateral load for zero axial load, $f'_c = 27.5$ MPa, $f_y = 260$ MPa.

compressive force increases, the depths to the neutral axes in the steel faceplates and the infill concrete from the extreme fibers in compression both increase, which is an expected result.

Fig. 10 presents the effect of reinforcement ratio on the vertical stress profile in the steel faceplates. The slope of the stress profile on the tension side of the steel faceplates decreases as the reinforcement ratio increases. The depth to the neutral axis in the steel faceplates also increases as the reinforcement ratio increases.

The finite element analysis results were used to aid the derivation of a mechanics-based predictive equation for the flexural capacity of SC wall piers. Fig. 11 presents the strain and stress profiles in the steel faceplates and infill concrete used in the derivation

The vertical stress distributions predicted by LS-DYNA in the infill concrete and steel faceplates at the base of the SC walls with different aspect ratios, reinforcement ratios, and axial load ratios were used to propose expressions for modification factors λ_1, λ_2, and λ_3. The effect of moment-to-shear ratio on the maximum strain in the extreme fiber in compression, ε_c, is given by λ_1:

$$\lambda_1 = \frac{M/VL - 0.3}{1.2} \tag{9}$$

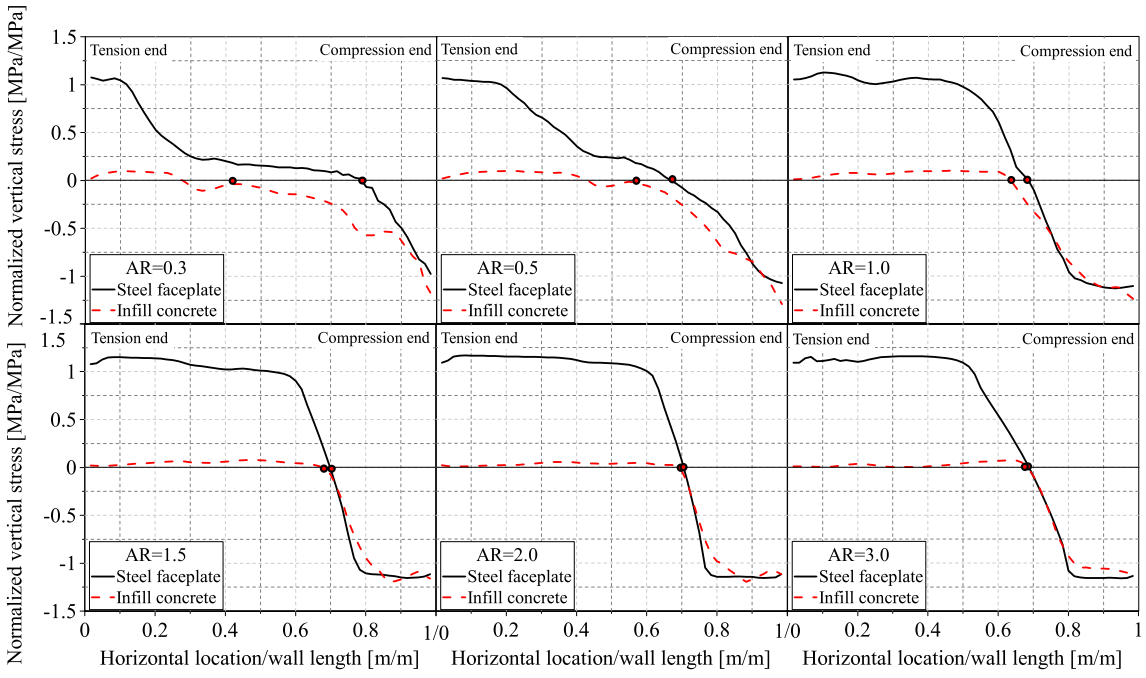

Fig. 9. DYNA-predicted normal stress in steel faceplates and infill concrete at peak strength for an axial load ratio of 0.2, $f'_c = 27.5$ MPa, $f_y = 260$ MPa.

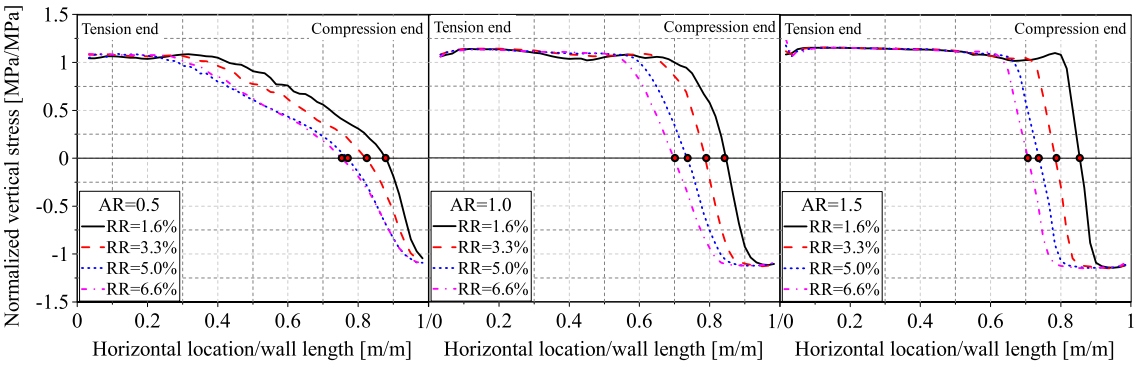

Fig. 10. Effect of reinforcement ratio on the steel normal stress profile at the wall base.

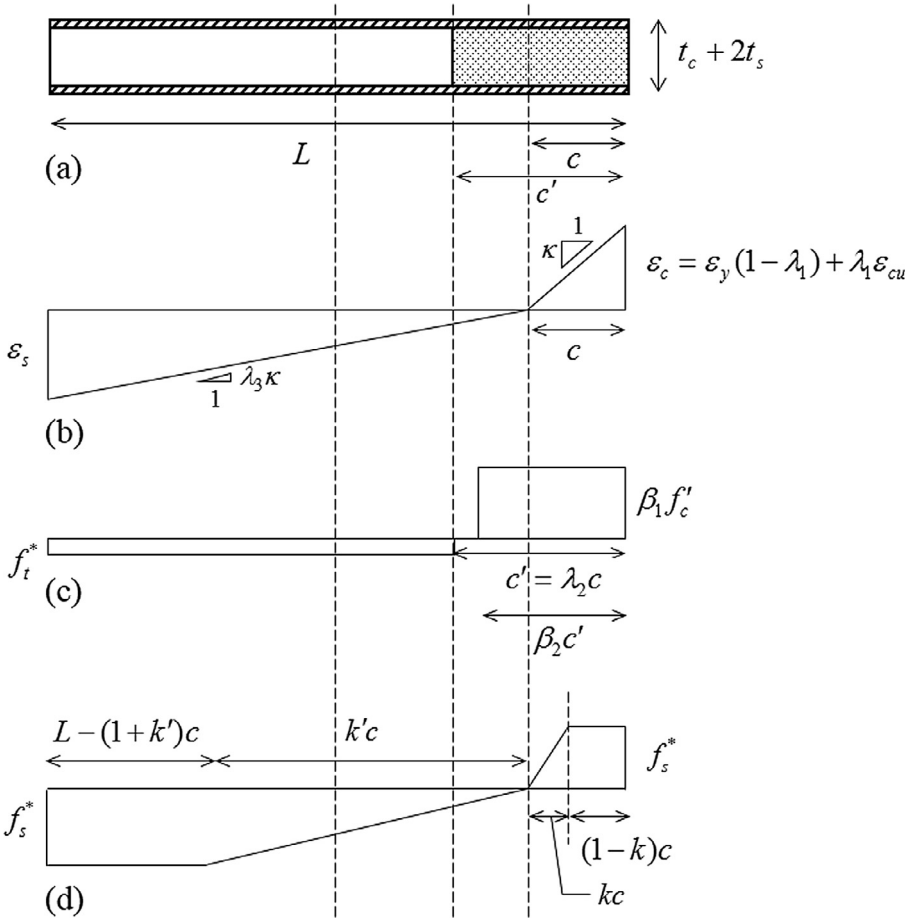

Fig. 11. Moment capacity calculation; (a) SC wall cross section; (b) vertical strain profile; (c) vertical stress profile in infill concrete; and (d) vertical stress profile in steel faceplates.

where M/VL is the normalized moment-to-shear ratio, noting that the normalized moment-to-shear ratio is identical to the wall aspect ratio, H/L, for a single story wall panel. The numerical analysis results indicated that the neutral axis in the steel faceplates and infill concrete are not collocated for low-aspect ratio SC walls. The difference between the neutral axis depths of the infill concrete and steel faceplates, c' and c in Fig. 11 respectively, is given by parameter λ_2:

$$\lambda_2 = 1.42(M/VL)^{-0.86} \quad (10)$$

The difference between c' and c decreases as M/VL increases and they are effectively identical for $M/VL \geqslant 1.5$.

As seen in Figs. 8 and 9, the vertical stress and strain do not distribute linearly along the length of the wall due to shear-flexure interaction, and the assumption of plane sections remaining plane after bending is violated. On the basis of the results of the finite element analyses, the strain variation for low aspect ratio SC wall piers can be represented by the bi-linear relationship shown in Fig. 11b. The slope of the strain profile on the tension side is a function of aspect ratio, axial load ratio, and reinforcement ratio. The

effect of these parameters on the slope of the stress profile is considered by parameterλ_3:

$$\lambda_3 = \left(1 + \frac{N}{0.2f'_cA_g}\left(1.21(M/VL)^{-0.48} - 1\right)\right)(0.05\exp(2M/VL))(0.17\rho_s + 0.75) \leqslant 1.0 \quad (11)$$

The strain profile is linear for SC walls with an aspect ratio of 1.5 and greater.

The parameter ε_c is varied from the yield strain of the steel faceplates to the ultimate strain of the infill concrete (=0.004) as the aspect ratio increases from 0.3 to 1.5, and it remains constant for aspect ratios greater than 1.5:

$$\varepsilon_c = \varepsilon_y(1 - \lambda_1) + \varepsilon_{cu}\lambda_1 \quad (12)$$

Parameters λ_1, λ_2, and λ_3 are each equal to 1.0 for $M/VL \geqslant 1.5$. Given the values of the parameters λ_1, λ_2, and λ_3 from Eqs. (9)–(11) and ε_c from Eq. (12), the depth to the neutral axis can be calculated as:

$$c = \frac{\frac{N}{A_sf_y} + 1 + \varphi'}{\lambda_2(\varphi + \varphi') + k(1 - \lambda_3)/(2\lambda_3) + 2} \quad (13)$$

where

$$\varphi = \frac{\beta_1\beta_2f'_c}{\rho_sf^*_s} \quad (14)$$

Table 7
Values of the stress block parameters.

ε_c	β_1	β_2
0.001	0.55	0.70
0.0015	0.75	0.72
0.002	0.88	0.75
0.0025	0.94	0.78
0.003	0.96	0.81
0.0035	0.97	0.83
0.004	0.98	0.85

$$\varphi' = \frac{f^*_t}{\rho_sf^*_s} \quad (15)$$

$$k = \frac{\varepsilon_y}{\varepsilon_c} \quad (16)$$

Given the value of c and setting $\alpha = c/L$, $\lambda_{3\,\min}$ is:

$$\lambda_{3\,\min} = \frac{\varepsilon_y\alpha}{(1 - \alpha)\varepsilon_c} \quad (17)$$

If $\lambda_3 < \lambda_{3\,\min}$, c needs to be re-calculated assuming $\lambda_3 = \lambda_{3\,\min}$.

The values of the stress block parameters, β_1 and β_2 in Eq. (14), are calculated assuming that the equivalent rectangular stress block recovers the area under the concrete stress-strain relationship and the location of its resultant, respectively. Table 7 lists the values these stress block parameters as a function of ε_c. The concrete stress-strain relationship proposed by Tsai [39] was used to calculate the stress block parameters.

The bending moment capacity of an SC wall pier can then be calculated as:

$$M_u = \beta_1\beta_2f'_cA_cL_c + A_sf^*_sL_s + A_cf^*_tL'_c \quad (18)$$

where

$$L_c = L[\lambda_2\alpha(1 - \beta_2\lambda_2\alpha)/2] \quad (19)$$

$$L'_c = L[\lambda_2\alpha(1 - \lambda_2\alpha)/2] \quad (20)$$

$$L_s = \alpha L[1 + 0.25k(1/\lambda_3 - 1) - \alpha(1 + 0.5k(1/\lambda_3 - 1) + k^2(1/\lambda_3^2 + 1)/6))] \quad (21)$$

Numerical analyses indicated that as the aspect ratio increases, the vertical strain in the steel faceplates and infill concrete increases, leading to an increase in the vertical stress in the faceplates due to hardening and to a reduction in the tensile stress in the infill concrete due to cracking. On the basis of the finite element analysis results, the effective stress in the steel faceplates, f^*_s, and the effective tensile strength of the infill concrete, f^*_t, can be calculated as:

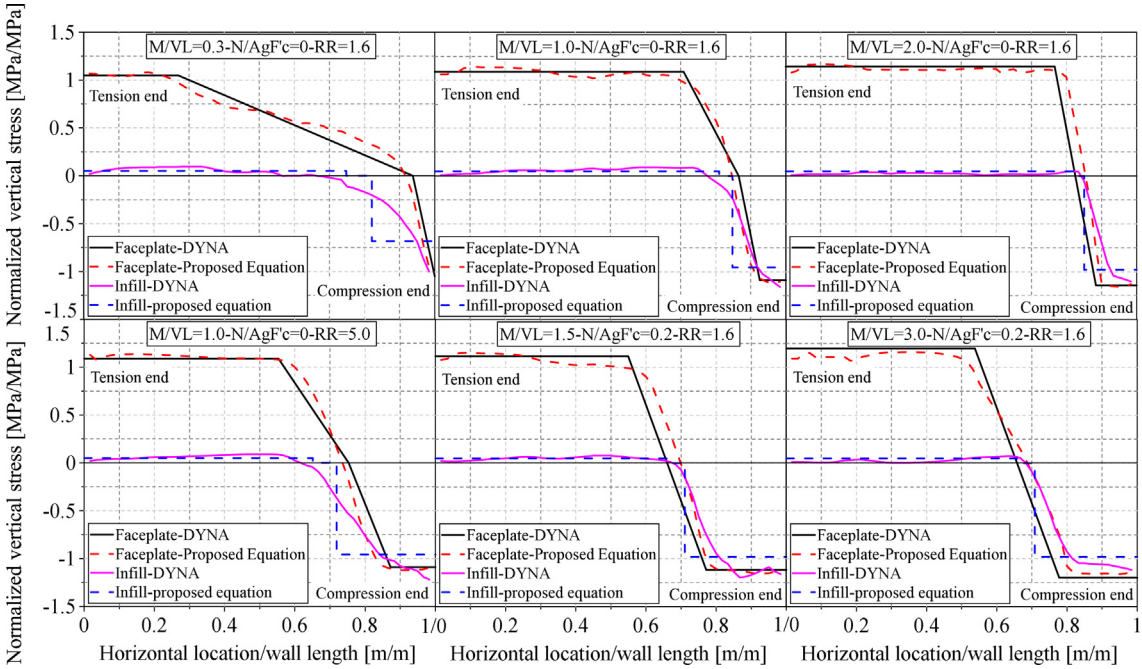

Fig. 12. LS-DYNA and model predicted responses.

$$1.05f_y \leqslant f_s^* = [1.05 + 0.056(M/VL - 0.3)]f_y \leqslant 1.2f_y \quad (22)$$

$$0 \leqslant f_t^* = 0.185(3 - M/VL)f \leqslant 0.5f_t \quad (23)$$

Given the bending moment capacity, the lateral load capacity of SC walls can be calculated as:

$$V_u = \frac{M_u}{H^*} \quad (24)$$

Fig. 13 presents a flowchart for the calculation of the moment capacity of an SC wall pier.

6.2. Verification of the proposed equations

Fig. 12 presents the DYNA-predicted normal stress profiles in the steel faceplates and infill concrete at peak lateral load together with those predicted using the Eqs. (9)–(17). As seen in Fig. 12, the

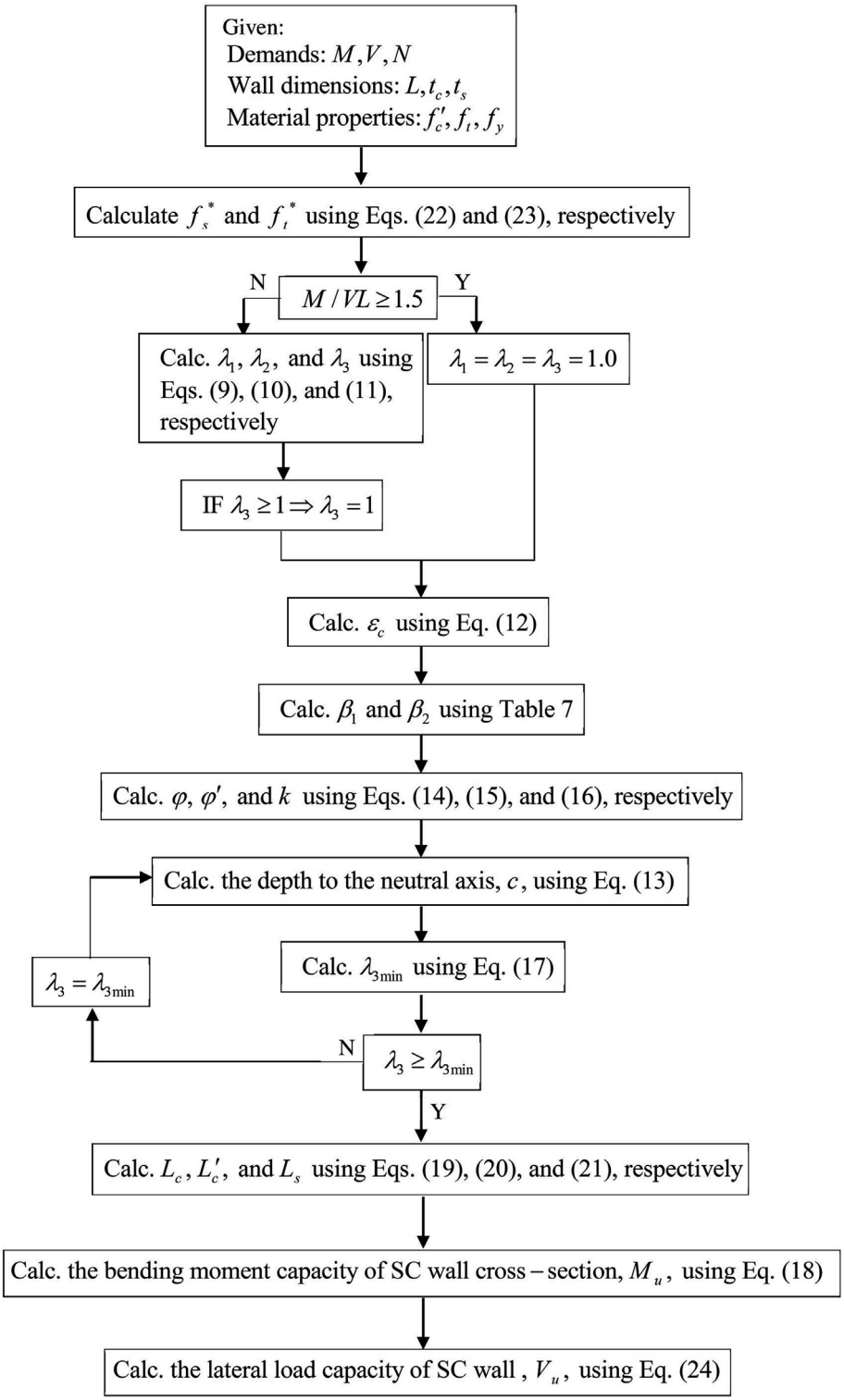

Fig. 13. Lateral load capacity calculation for SC wall piers.

Table 8
Predicted lateral load capacities.

AR	AL	RR (%)	Predicted lateral load capacity (kN)		Ratio
			LS-DYNA	Mechanics-based Eq. (24)	
0.3	0	1.6	2954	3083	0.96
0.3	0.2	1.6	4070	4662	0.87
0.5	0	1.6	2282	2037	1.12
0.5	0	3.3	3474	3172	1.10
0.5	0	5	4404	4168	1.06
0.5	0	6.6	4404	5093	0.86
0.5	0.2	1.6	3358	3207	1.05
1	0	1.6	1117	1094	1.02
1	0	3.3	1953	1886	1.04
1	0	5	2736	2535	1.08
1	0	6.6	3479	3145	1.11
1	0.2	1.6	1882	1766	1.07
1.5	0	1.6	725	747	0.97
1.5	0	3.3	1228	1210	1.01
1.5	0	5	1677	1632	1.03
1.5	0	6.6	2117	2024	1.05
1.5	0.2	1.6	1237	1205	1.03
2	0	1.6	512	569	0.90
2	0.2	1.6	912	912	1.00
3	0	1.6	320	356	0.90
3	0.2	1.6	574	618	0.93

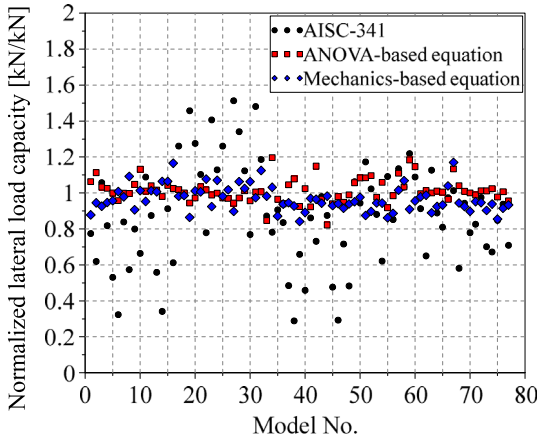

Fig. 14. Predicted normalized lateral load capacity of the SC walls.

proposed equations accurately predict the normal stress variation in the steel faceplates and infill concrete of SC walls with different moment-to-shear, reinforcement, and axial load ratios. The locations of the neutral axes and change in the slope of the normal stress profile on the tension and compression sides of the steel faceplates predicted by the proposed equations match the DYNA-predicted results.

The DYNA- and mechanics-based-predicted lateral load capacities of the SC walls with different aspect ratio, reinforcement ratio, and axial load ratio are listed in Table 8. The mechanics-based-predicted lateral load capacities, listed in Table 8, were calculated using Eq. (24). The lateral load capacities of the SC walls are predicted with an error of less than 15%. The lateral load capacity is significantly underestimated if the tensile strength of the infill concrete is ignored.

7. Verification and validation of the mechanics-based and ANOVA-based equations

Two sets of data are used to verify and validate the proposed mechanics-based and ANOVA-based equations for peak resistance of an SC wall pier: LS-DYNA analysis and data from tests of four SC walls with an aspect ratio of 0.5.

7.1. Verification

The results of analysis of the 77 LS-DYNA models presented in Table 4 are used to validate the ANOVA-based and mechanics-based equations. Fig. 14 presents three normalized lateral load capacities for each of 77 models. The normalized lateral load capacities were estimated by dividing the lateral load capacity calculated based on (1) ANOVA-based Eq. (2), (2) mechanics-based Eq. (24), and (3) specifications of AISC 341-16 [40], to the DYNA-predicted peak load. The draft Standard AISC 341-16 [40], includes provisions for design of composite plate shear walls: concrete filled (C-PSW/CF). Section H7.5a of AISC 341-16 specifies that the nominal moment capacity of C-PSW/CF without boundary elements be calculated as the moment corresponding to yielding of the steel faceplates in flexural tension and first yield in flexural compression assuming a linear elastic stress distribution, a maximum concrete compressive stress equal to $0.7f'_c$, and maximum steel stress equal to f_y.

The ratio of lateral load capacity predicted by the ANOVA-based Eq. (2) and the mechanics-based Eq. (24) to the DYNA-predicted peak load varies from 0.82 to 1.2, indicating that both equations reasonably recover the numerically predicted lateral load capacity. We consider this outcome to verify the mechanics-based design equation.

There are significant differences between the AISC- and numerically-predicted lateral load capacities because the proposed AISC equations ignore the effects of wall aspect ratio, reinforcement ratio, and axial load.

7.2. Validation

Data from the in-plane testing of SC walls by Chen [38,41] are used for further independent validation of the accuracy of the mechanics-based and ANOVA-based models. Data from the tests at the University at Buffalo were not utilized for this purpose because they were used to validate the LS-DYNA model.

Chen [38,41] tested four low-aspect ratio SC walls under displacement-controlled cyclic loading. The aspect ratio of the four walls was 0.5. The height and the length of the walls were 1220 mm and 2000 mm, respectively. The distance between the wall base and the center line of the loading plates was 1000 mm. The steel faceplates were embedded into the foundation block using shear studs

Fig. 15. SC1 specimen before the test [10].

attached to the inside of the steel plates. Holes in the steel faceplates enabled the placement of transverse reinforcement in the foundation block. The total wall thickness was 290 mm for SC1 and SC2 and 200 mm for SC3 and SC4. The faceplates were 4.5-mm thick, yielding reinforcement ratios of 3.1% and 4.5% for SC1/SC2 and SC3/SC4, respectively. The diameter of the studs and tie rods was 13 mm. Studs and tie rods were used in SC1 and SC3 but only tie rods were used in SC2 and SC4. The studs were spaced 75 mm on center in SC1 and SC3. Tie rods were spaced at 150 mm in all SC walls. A photograph of SC1 is presented in Fig. 15. More information about the material properties, test setup, loading protocol, and instrumentation are reported in Chen [38,41].

Fig. 16 presents the measured first-quadrant cyclic force-displacement relationships (solid gray line) for the walls tested

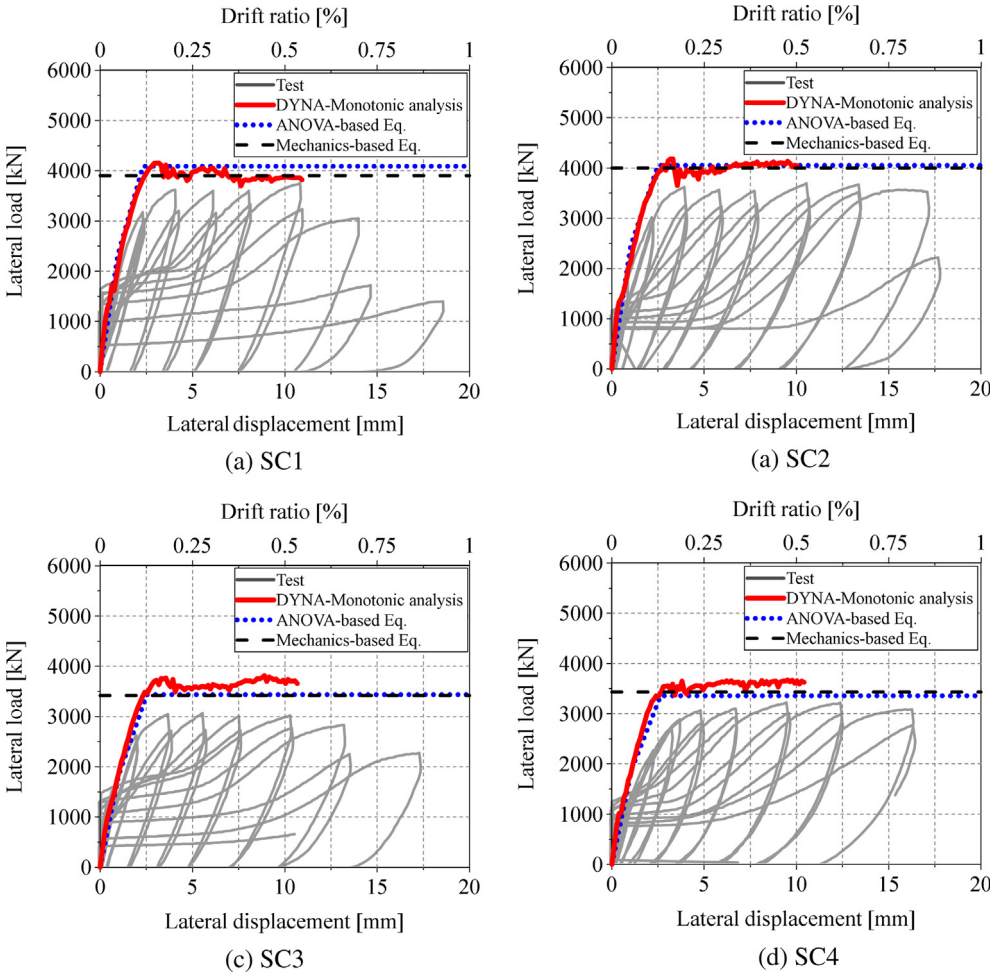

Fig. 16. Predicted and measured responses of the SC walls.

by Chen, the mechanics-based lateral strengths per Eq. (24) (dashed black line), ANOVA-based prediction of monotonic response per Eqs. (1)–(7) (dotted blue[1] line), and the LS-DYNA-predicted monotonic response (solid red line). The LS-DYNA analyses of Chen's walls were performed using the same material models, elements, and boundary conditions used for the analysis of 77 SC wall piers described previously.

The predictive equations, proposed in this study for response under monotonic loading, slightly overestimate the cyclic response of Chen's walls [41], which is an expected outcome. Fig. 16 shows that the ANOVA-based predictions of monotonic response and the mechanics-based predictions of peak strength agree well with the monotonic responses predicted by analysis of the LS-DYNA models.

8. Summary and conclusions

The effects of key design variables on the in-plane response of SC wall piers without boundary elements were studied systematically and results were used to develop predictive equations for the monotonic lateral force- displacement relationship up to peak strength, and a mechanics-based equation for the lateral load capacity, of SC wall piers. The general-purpose finite element code LS-DYNA was used for the simulations. The baseline model was validated in a prior study by the authors for calculations of in-plane, inelastic cyclic response, using data from tests of large-size wall piers.

The design variables considered in this study included wall aspect ratio ranging from 0.3 to 3.0, reinforcement ratio ranging from 1.6% to 6.6%, slenderness ratio ranging from 10 to 50, axial load ratio ranging from 0 to 0.2, steel strength ranging from 235 to 460 MPa, and concrete strength ranging from 27 to 55 MPa.

Statistical analyses were performed to investigate the main and interaction effects of the key design variables on the lateral strength and stiffness of SC walls using a three-level fractional factorial design method. Lateral load capacity and stiffness are affected significantly by aspect ratio. Although faceplate slenderness ratio had the smallest effect on strength and initial stiffness, it has a marked effect on post-yield stiffness: the greater slenderness ratio, the lower the post-yield stiffness. Aspect ratio has a substantial impact on global response; as it increases, the effects of other design variables on strength and stiffness decrease.

The results of the LS-DYNA analyses were used to develop a trilinear relationship for the monotonic response of an SC wall pier up to peak strength. The adequacy of the proposed relationship was verified by examining the independency and normal distribution of the residuals.

A mechanics-based equation was developed for predicting the bending moment capacity of an SC wall pier considering the co-existing shear and axial forces, and the effects of aspect ratio, axial load, and reinforcement ratio. Importantly, this study showed that the bending-moment capacity of SC wall piers cannot be predicted accurately by equation proposed in ASIC 341 because the effects of key design variables and the axial force-shear force interaction are ignored.

The proposed mechanics-based and ANOVA-based equations were verified and validated using finite element analysis results and data from tests of four low-aspect ratio SC wall piers at National Taiwan University. The DYNA-predicted peak load of 77 SC walls with various design variables and the in-plane monotonic response up to peak load of the tested SC walls were successfully predicted using the proposed equations.

[1] For interpretation of color in Fig. 16, the reader is referred to the web version of this article.

The proposed mechanics-based and ANOVA-based equations are applicable for the range of design variables considered in this study. Further studies are needed to expand the ranges of the design variables and to address SC walls with boundary columns and flanges.

Acknowledgements

This project was supported in part by the US National Science Foundation under Grant No. CMMI-0829978. This support is gratefully acknowledged. The authors thank Mr. P. Chen and Professor Yin-Nan Huang at the National Taiwan University for providing data from their tests of SC walls that were used for the validation study presented in the paper.

References

[1] Akita S, Ozaki M, Niwa N, Matsuo I, Hara K. Study on steel plate reinforced concrete bearing wall for nuclear power plants (part #2): analytical method to evaluate response of SC walls. In: 22nd International conference on structural mechanics in reactor technology (SMiRT16). Washington (DC, USA): International Association for Structural Mechanics in Reactor Technology (IASMiRT); 2001.
[2] Akiyama H, Sekimoto H, Tanaka M, Inoue K, Fukihara M, Okuda Y. 1/10th scale model test of inner concrete structure composed of concrete filled steel bearing wall. In: 10th International conference on structural mechanics in reactor technology (SMiRT10). Anaheim (CA, USA): International Association for Structural Mechanics in Reactor Technology (IASMiRT); 1989. p. 73–8.
[3] Bowerman H, Coyle N, Chapman JC. An innovative steel/concrete construction system. Struct Eng 2002;80:33–8.
[4] Chaudhary S, Ali A, Kim D, Cho SG. Seismic analysis of steel concrete composite walls of nuclear power plant structures. In: 21th International conference on structural mechanics in reactor technology (SMiRT21). New Delhi (India): International Association for Structural Mechanics in Reactor Technology (IASMiRT); 2011.
[5] Danay A. Response of steel-concrete composite panels to in-plane loading. Nucl Eng Des 2012;242:52–62.
[6] Emori K. Compressive and shear strength of concrete filled steel box wall. Steel Struct (Kor J) 2002;2:29–40.
[7] Eom TS, Park HG, Lee CH, Kim JH, Chang IH. Behavior of double skin composite wall subjected to in-plane cyclic loading. J Struct Eng 2009;135:1239–49.
[8] Epackachi S. Experimental, numerical, and analytical studies on the seismic response of steel-plate concrete (SC) composite shear walls Buffalo [Ph.D. Dissertation]. Buffalo (NY): University at Buffalo; 2014.
[9] Epackachi S, Whittaker AS. Experimental, numerical, and analytical studies on the seismic response of steel-plate concrete (SC) composite shear walls [MCEER Technical Report 16–0001]. Buffalo (NY): University at Buffalo; 2016.
[10] Epackachi S, Nguyen NH, Kurt EG, Whittaker AS, Varma AH. In-plane seismic behavior of rectangular steel-plate composite wall piers. J Struct Eng 2014;141:04014176-1–176-9.
[11] Epackachi S, Whittaker AS, Huang YN. Analytical modeling of rectangular SC wall panels. J Constr Steel Res 2014;105:49–59.
[12] Kurt EG, Varma AH, Booth P, Whittaker AS. In-plane behavior and design of rectangular sc wall piers without boundary elements. J Struct Eng 2016;142:04016026-1–04016026-16.
[13] Nie JG, Hu HS, Fan JS, Tao MX, Li SY, Liu FJ. Experimental study on seismic behavior of high-strength concrete filled double-steel-plate composite walls. J Constr Steel Res 2013;88:206–19.
[14] Ozaki M, Akita S, Niwa N, Matsuo I, Usami S. Study on steel plate reinforced concrete bearing wall for nuclear power plants part 1: shear and bending loading tests of SC walls. In: 16th International conference on structural mechanics in reactor technology (SMiRT16). Washington (DC, USA): International Association for Structural Mechanics in Reactor Technology (IASMiRT); 2001.
[15] Sener KC, Varma AH. Steel-plate composite walls: experimental database and design for out-of-plane shear. J Constr Steel Res 2014;100:197–210.
[16] Suzuki N, Akiyama H, Narikawa M, Hara K, Takeuchi M, Matsuo I. Study on a concrete filled steel structure for nuclear power plants (part #4): analytical method to estimate shear strength. In: 13th International conference on structural mechanics in reactor technology (SMiRT13). Porto Alegre (Brazil): International Association for Structural Mechanics in Reactor Technology (IASMiRT); 1995. p. 33–8.
[17] Usami S, Akiyama H, Narikawa M, Hara K, Takeuchi M, Sasaki N. Study on a concrete filled steel structure for nuclear power plants (part #2): compressive loading tests on wall members. In: 13th International conference on structural mechanics in reactor technology (SMiRT13). Porto Alegre (Brazil): International Association for Structural Mechanics in Reactor Technology (IASMiRT); 1995. p. 21–6.
[18] Varma AH, Malushte SR, Sener KC, Lai Z. Steel-plate composite (SC) walls for safety related nuclear facilities: design for in-plane forces and out-of-plane moments. Nucl Eng Des 2014;269:240–9.

[19] Vecchio F, McQuade I. Towards improved modeling of steel-concrete composite wall elements. Nucl Eng Des 2011;241:2629–42.
[20] Zhao Q, Astaneh-Asl A. Cyclic behavior of traditional and innovative composite shear walls. J Struct Eng 2004;130:271–84.
[21] Fukumoto T, Kato B, Sato K. Concrete filled steel bearing walls. IABSE report; 1987.
[22] Takeda T, Yamaguchi T, Nakayama T, Akiyama K, Kato Y. Experimental study on shear characteristics of concrete filled steel plate wall. In: 13th International conference on structural mechanics in reactor technology (SMiRT13). Porto Alegre (Brazil): International Association for Structural Mechanics in Reactor Technology (IASMiRT); 1995. p. 3–14.
[23] Sasaki N, Akiyama H, Narikawa M, Hara K, Takeuchi M, Usami S. Study on a concrete filled steel structure for nuclear power plants (part #2): shear and bending loading tests on wall member. In: 13th International conference on structural mechanics in reactor technology (SMiRT13). Porto Alegre (Brazil): International Association for Structural Mechanics in Reactor Technology (IASMiRT); 1995. p. 27–32.
[24] Jian-Guo N, Hong-Song H, Jian-Sheng F, Mu-Xuan T, Sheng-Yong L, Fu-Jun L. Experimental study on seismic behavior of high-strength concrete filled double-steel-plate composite walls. J Constr Steel Res 2013;88:206–19.
[25] SIMULIA. Abaqus Analysis User's Manual, Version 6.12. Providence (RI, USA): Dassault Systèmes Simulia Corp.; 2012.
[26] Epackachi S, Whittaker AS, Varma AH, Kurt EG. Finite element modeling of rectangular steel-plate composite shear walls. Eng Struct 2015;100:369–84.
[27] LS-DYNA. Keyword user's manual, version 971 R6.0.0, vo. I. Livermore (CA, USA); 2012.
[28] LS-DYNA. Keyword user's manual, Version 971 R6.0.0, vol. II. Livermore (CA, USA); 2012.
[29] ACI 318 Committee. Building code requirements for structural concrete (ACI 318-14) and commentary. Farmington Hills (MI): American Concrete Institute; 2014.
[30] Ozcebe G, Saatcioglu M. Hysteretic shear model for reinforced concrete members. J Struct Eng 1989;115:132–48.
[31] Baltay P, Gjelsvik A. Coefficient of friction for steel on concrete at high normal stress. J Mater Civ Eng 1990;2:46–9.
[32] Rabbat BG, Russell HG. Friction coefficient of steel on concrete or grout. J Struct Eng 1985;111:505–15.
[33] Han LH, He SH, Liao FY. Performance and calculations of concrete filled steel tubes (CFST) under axial tension. J Constr Steel Res 2011;67:1699–709.
[34] Moon J, Roeder CW, Lehman DE, Lee H-E. Analytical modeling of bending of circular concrete-filled steel tubes. Eng Struct 2012;42:349–61.
[35] Montgomery DC. Design and analysis of experiments. 4th ed. New York: Wiley; 1982.
[36] Chadwell CB, Imbsen RA. XTRACT-cross section analysis software for structural and earthquake engineering. Rancho Cordova (CA): TRC; 2002.
[37] Minitab. Minitab Manual. Minitab Inc.; 2013.
[38] Chang CC, Huang YN, Chen BA, Epackachi S, Whittaker A. An experimental study for in-plane cyclic behavior of low aspect-ratio steel-concrete composite walls. In: 23rd International conference on structural mechanics in reactor technology (SMiRT 23). Manchester (UK): International Association for Structural Mechanics in Reactor Technology (IASMiRT); 2015.
[39] Tsai WT. Uniaxial compressional stress-strain relation of concrete. J Struct Eng 1988;114:2133–6.
[40] American Institute of Steel Construction. Seismic provisions for structural steel buildings (AISC341), Chicago, IL; 2016.
[41] Chen PA. An experimental study of the in-plane cyclic behavior of low-aspect-ratio steel-plate composite walls [Master Thesis]. Taiwan: National Taiwan University; 2015.